

ELECTROSTATIC INTERACTION BETWEEN LONG, RIGID HELICAL MACROMOLECULES AT ALL INTERAXIAL ANGLES

A. A. Kornyshev

*Institute for Theoretical Physics, University of California at Santa Barbara, USA; and Research Center
"Jülich", D-52425 Jülich, Germany*

S. Leikin^{*}

*Laboratory of Physical and Structural Biology, National Institute of Child Health and Human
Development, National Institutes of Health, Bethesda, MD 20892, USA*

^{*} To whom reprint requests should be addressed. LPSB/NICHD, Bldg. 12A, Rm. 2041, NIH, Bethesda,
MD 20892, USA; e-mail leikin@helix.nih.gov; FAX 1-301-496-2172.

ABSTRACT

We derive formulae for the electrostatic interaction between two long, rigid macromolecules that may have arbitrary surface charge patterns and cross at an arbitrary interaxial angle. We calculate the dependence of the interaction energy on the interaxial angle, on the separation, and on the precise alignment of the charge pattern on one molecule with respect to the other. We focus in particular on molecules with helical charge patterns. We report an exact, explicit expression for the energy of interaction between net-neutral helices in a nonpolar medium as well as an approximate result for charged helices immersed in an electrolyte solution. The latter result becomes exact in the asymptotic limit of large separations. Molecular chirality of helices manifests itself in a torque that tends to twist helices in a certain direction out of parallel alignment and that has a nontrivial behavior at small interaxial angles. We illustrate the theory with the calculation of the torque between layers of idealized, DNA-like double helices in cholesteric aggregates. We propose a mechanism of the observed cholesteric-to-columnar phase transition and suggest an explanation for the observed macroscopic (0.4-5 μm) pitch of the cholesteric phase of *B*-DNA.

I. INTRODUCTION

Assemblies of long helical macromolecules are common building blocks of living organisms. Bundles of α -helices form domains in many proteins. Bundles of triple-helical collagen form tendons, ligaments, cornea, matrix of skin and bone, and other connective tissue structures. DNA is often stored inside cells and viral capsids in the form of dense aggregates. In other words, many biological interactions involve helices and many complex biological structures consist of helices.

All helices are chiral, i.e. the mirror image of a right-handed helix is left-handed and vice versa. Biological helices manifest their chirality by twisting with respect to each other. Specifically, α -helices form bundles and coiled coils where their long axes cross at a small angle. DNA forms a cholesteric phase that consists of molecular layers. The molecules are parallel within each layer, but their principle axis rotates from layer to layer by a small, constant angle, typically a fraction of a degree [1-6]. Similar assemblies are formed by α -helices in organic solvents [1,7,8], by collagen at low pH [9], and by a variety of other helices. The direction and the amplitude of the twist in cholesteric phases, in helical bundles, and in coiled coils are not random. They are encoded in intermolecular interactions and they are always the same under similar conditions.

The relationship between the twist and the molecular structure is not trivial and still not understood. Some of the puzzles are: (a) reversal of the direction of the twist in the cholesteric phase that occurs upon variation in solvent composition even though the handedness of helices remains the same [7]; (b) dependence of the amplitude of the twist on the interaxial separation between helices [7,8,10]; (c) phase transitions in assemblies of helices, e.g. the transition from a non-chiral line hexatic phase to the chiral cholesteric phase [11,12]; (d) anomalously small interaxial angles between helices in the cholesteric phase that could not be justified in terms of structural and dimensional arguments [1-11,13,14]. The solution of these puzzles is likely to be based on understanding properties of chiral interaction potentials between helices at nonzero interaxial angles [15]. Creation of a rigorous theory for such interaction is believed to be one of the biggest challenges of the physics of molecular chirality [15,16].

Electrostatics is a major component of interaction between biological helices since virtually all of them have high density of surface charges. For instance, DNA has an elementary charge per each 1.7 Å of its axial length. As a result, interactions between DNA helices in aggregates are primarily electrostatic. Backbone of an α -helix contains a negatively charged carbonyl oxygen and a positively charged amide hydrogen per each 3-4 Å of axial length. The spiral of carbonyls and amides produces an electric field that exponentially decays away from it with the characteristic length \sim 1 Å. The electrostatic interaction between neighboring α -helices in a bundle may be quite strong because of their close contact and their low dielectric constant.

Fifty years ago, a formula for the energy of electrostatic interaction between crossed, homogeneously charged rods was derived by Onsager based on the Derjaguin approximation [17]. Twenty five years later, a more general result for the same problem was obtained by Brenner and Parsegian [18] without using the Derjaguin approximation. However, homogeneously charged rods are not chiral and, therefore, these results do not tell us anything about the chiral potential. Further progress was impeded by the absence of a mathematical formalism appropriate for chiral helical macromolecules.

To address the effects of molecular chirality, one must take into account the helical structure of a surface charge pattern and its handedness. Electrostatic models for an isolated, charged spiral in an electrolyte solution were recently reported in [19-23]. In particular, the electrostatic potential, counterion distribution around DNA, and the transition between the *B* and *A* forms of DNA in solution were discussed. Electrostatic interactions between several helices that have parallel long axes were calculated in [24]. It was suggested that various details of the helical symmetry of DNA surface charge pattern may be responsible for such observed phenomena as: DNA overwinding from \sim 10.5 base pairs (bp) per turn in solution to 10 bp/turn in fibers [25], meso- and poly-morphism of DNA in dense aggregates [26], and DNA condensation by counterions [27]. However, none of these results can be directly applied to intermolecular interaction in chiral aggregates (twisted bundles and the cholesteric phase) where molecular axes cross at a non-zero angle.

Development of a theory for electrostatic interactions between long, chiral macromolecules at all interaxial angles is the subject of the present work. First, we derive a result that is valid at arbitrary charge distributions on molecular surfaces. Next, we apply this result to molecules whose surface charge patterns have basic helical symmetries. At the present stage, we incorporate only the most simple, but essential elements of helical structure. We assume that molecules are rigid rods that have helical surface charge patterns. We model a spiral string of point charges by a continuous spiral line charge with the appropriate charge density, helical pitch, and handedness.

Imperfections of molecules and thermal motions are not included into the model. This is not because we believe that the corresponding details are not important, but because one can hope to understand the reality only after thoroughly examining the most simple “ground state” of the system. Once we understand the basics, we will be able to build in details and investigate their role in each specific case.

In general, chiral phenomena are very complex. Each of them deserves a separate, dedicated discussion, because different details are important in each case. Here we focus primarily on laying out the background for the theory. For illustration, we consider interaction between 150 bp *B*-DNA fragments that can be roughly approximated as rigid rods. We suggest how different observed features of the cholesteric phase formed by such DNA fragments can be qualitatively deduced from properties of the chiral interaction potential between them.

The paper is structured as follows. In Section II, we define the model. In Section III, we present general formulae for the energy of interaction between molecules with helical surface charge patterns and consider simple limiting cases. In Section IV, we discuss interaction between infinitely long helices at small interaxial angles and large separations. In Section V, we show how the results derived for infinitely long helices can be modified and applied to a more realistic case of interaction between two helices of finite length. In Section VI, we analyze main qualitative features expected and observed in the cholesteric phase of 150 bp DNA. All algebra is reported in the Appendix where we derive formulae for the energy of interaction between two molecules with arbitrary surface charge distribution at an arbitrary interaxial angle and apply these formulae to molecules with helical charge patterns.

II. THE MODEL

We consider interaction between two long, rigid molecules whose axes cross at an arbitrary angle ψ and are separated by the distance R at the point of their closest approach. The configuration and coordinate systems are shown schematically in Fig. 1. The molecules have cylindrical, dielectric inner cores. They are immersed either in an electrolyte solution or in a nonpolar medium. Their intrinsic surface charges form arbitrary, inhomogeneous patterns at surfaces of the inner cores.

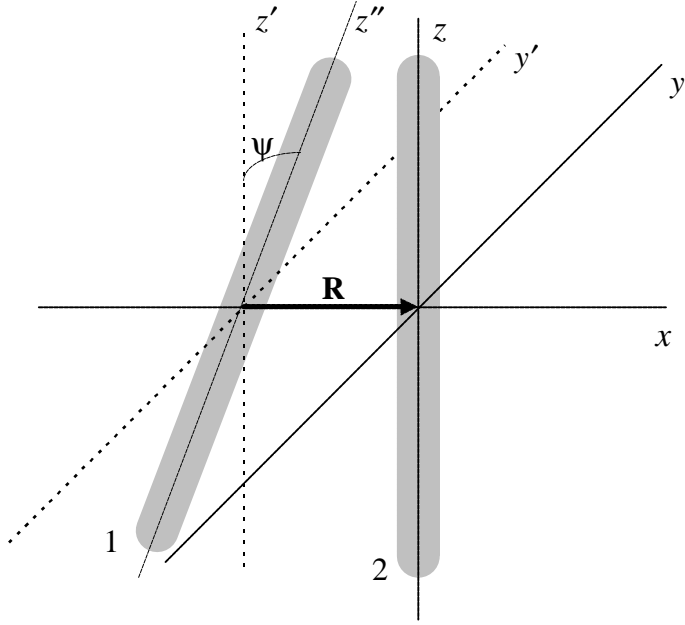


Fig. 1. Configuration of two molecules (1,2) twisted with respect to each other by an *interaxial angle* ψ and shifted by a vector \mathbf{R} connecting two points of the closest approach on molecular axes. We use three Cartesian coordinate systems: (i) the laboratory frame (x,y,z) whose z -axis coincides with the long axis of molecule 2 and x -axis goes through the points of closest approach on the axes of molecules 1 and 2; (ii) the shifted laboratory frame (x',y',z') translated by the vector $-\mathbf{R}$ relative to (x,y,z); and (iii) the molecular frame (x'',y'',z'') whose z'' -axis coincides with the long axis of molecule 1 and x'' -axis is coaxial with the x -axis of the laboratory frame. The y'' -axis is not shown to avoid overloading the sketch. In addition to the Cartesian frames, we use two cylindrical molecular frames, each coaxial with the long axis of the corresponding molecule.

We calculate the electric field and the electrostatic interaction energy as a function of ψ and R and of the precise alignment of the charge pattern on one molecule with respect to the other. We start from the interaction Hamiltonian which is the energy at fixed surface charge patterns. Provided that the Hamiltonian for each isolated molecule is known [28], one can then determine the interaction *free energy* by averaging over fluctuations of surface charge densities. In the present work, however, we focus on a more simple case when one can substitute the averaged surface charge pattern into the interaction Hamiltonian to obtain the free energy. This can be done when the energy of *inter*-molecular interaction is much smaller than the *intra*-molecular energy and when the surface charge distributions do not undergo structural transitions,

triggered by intermolecular interaction. Such conditions are satisfied in the asymptotic limit of large intermolecular separations or when counterions are strongly bound (chemisorbed) at fixed positions on the surfaces. In these cases, the average surface charge pattern can either be calculated from an adsorption model or it can be approximated on the basis of semi-empirical considerations or computer simulations.

A. Debye-Hückel-Bjerrum approximation

Interaction in electrolyte solution. Many biological macromolecules, DNA in particular, have high density of surface charges. Under physiological conditions, they are surrounded by an ionic atmosphere with the Debye length $\lambda_D \sim 7 \text{ \AA}$. It is natural to expect here a nonlinear screening of fixed surface charges by electrolyte ions which is often treated within the mean-field, nonlinear Poisson-Boltzmann theory [29-31]. However, most of counterions which contribute to the nonlinear screening lie within a narrow layer around each molecule. We refer to them as condensed counterions. The thickness of this layer can be estimated as $d_c \leq A/4\pi l_B$, where A is the average area per elementary charge on the molecular surface and $l_B = e^2/\epsilon k_B T$ is the Bjerrum length ($\approx 7 \text{ \AA}$ in water). For most biological macromolecules $A \leq 100 \text{ \AA}^2$ and $d_c < 2 \text{ \AA}$. The thickness of this layer is comparable or even smaller than the size of a water molecule and than the characteristic roughness of the corrugated molecule/water interface. Mean-field description of an electric field inside such a thin layer is inappropriate.

We replace the Poisson-Boltzmann approximation by explicit treatment of condensed counterions. Specifically, we describe the molecular-core/water interface and the nonlinear screening layer as a single, infinitesimally thin surface that may have an arbitrary, inhomogeneous charge density. This surface contains fixed surface charges, chemisorbed ions, and mobile, condensed counterions. We describe the diffuse ionic atmosphere outside this surface within the Debye-Hückel theory [32]. This approach is similar to the *Debye-Hückel-Bjerrum* model which has proved to be quite successful in the theory of concentrated electrolyte solutions, including the theory of Coulomb criticality [33-36]. In our case, one may expect such model to be accurate as long as the ratio of d_c to all other characteristic lengths in the system (the Debye length, the surface-to-surface distance between the molecules, the helical pitch, etc.) is small.

Interaction in nonpolar medium. While nucleic acid helices (DNA or RNA) typically reside in aqueous electrolyte environment, many protein helices are immersed into nonpolar media. These may be α -helical domains inside a large globular protein or, e.g., transmembrane α -helices. Interaction between helical macromolecules in a nonpolar environment is relevant not only because of its potential biological applications, but also because of its conceptual importance. Indeed, lipid membranes and the interior of globular proteins have about the same dielectric constant as cores of α -helices, i.e. we can assume that the dielectric constant is the same everywhere. Furthermore, nonpolar media do not have dissolved electrolyte ions inside. This allows us to avoid approximations associated with interfaces between two different dielectrics and difficulties inherent to theories of electrolyte solutions. As a result, we can obtain *the exact* solution of the electrostatic problem as a particular case of the Debye-Hückel-Bjerrum model at $\kappa_D = 1/\lambda_D = 0$ and $\epsilon_c = \epsilon_s = \epsilon$, where ϵ_c is the dielectric constant of the molecular cores and ϵ_s is the dielectric constant of the solvent.

B. Surface charge patterns

We describe all charges at each molecular-core/water interface explicitly by their surface charge densities $\sigma_v(z, \phi)$, each in its own “molecular” frame of cylindrical coordinates. The index $v (= 1, 2)$ labels the two molecules. The z axis of each molecular frame coincides with the molecular axis; $z=0$ is the point of the closest approach between molecular axes; $\phi=0$ corresponds to the direction of the vector \mathbf{R} connecting the points of the closest approach on the axes of the two molecules (Fig. 1). In the Appendix, we derive a general relationship between the interaction energy and the cylindrical Fourier transforms of the surface charge densities $\tilde{\sigma}_v(q, n)$ that are defined as follows

$$\tilde{\sigma}_v(q, n) = \frac{1}{2\pi} \int_0^{2\pi} d\phi \int_{-\infty}^{\infty} dz \sigma_v(z, \phi) e^{in\phi} e^{iqz}, \quad (1)$$

$$\sigma_v(z, \phi) = \frac{1}{2\pi} \sum_{n=-\infty}^{\infty} \int_{-\infty}^{\infty} dq \tilde{\sigma}_v(q, n) e^{-in\phi} e^{-iqz}.$$

In the present work we focus on interaction between two identical helical macromolecules assuming that their surface charge densities obey the basic helical symmetry requirement

$$\sigma_v(z + \Delta z, \phi + g\Delta z) = \sigma_v(z, \phi), \quad (2)$$

where $g=2\pi/H$ for right-handed helices, $g=-2\pi/H$ for left-handed helices, and H is the helical pitch. Typically, this occurs when the charge density follows the underlying symmetry of the molecule. The surface charge density can, then, be rewritten in the form

$$\sigma_v(z, \phi) = \sigma_0 P(z - \phi/g + z_v). \quad (3)$$

Here $P(x)$ is a periodic function that defines the axial charge distribution,

$$P(x + Hk) = P(x); \quad (4)$$

z_v describes the axial position of each helix and it depends on the choice of a reference point; σ_0 is the mean surface density of dominant fixed charges. For example, DNA contains fixed phosphate charges and bound counterions so that σ_0 is the surface charge density of phosphates. Protein helices typically contain both negative and positive charges. If fixed charges of one sign dominate, we define σ_0 as their mean surface charge density. If a helix contains equal number of positive and negative charges, either one can be used to define σ_0 .

Within this definition, the mean surface charge density is

$$\bar{\sigma} = \sigma_0 \frac{1}{H} \int_0^H P(x) dx. \quad (5)$$

The cylindrical Fourier transform of $\sigma_v(z, \phi)$, defined by Eq. (3), gives

$$\sigma_v(q, n) = 2\pi \sigma_0 e^{ingz_v} p(q) \delta(q + ng), \quad (6)$$

where $\delta(x)$ is the Dirac's delta-function and

$$p(q) = \frac{1}{H} \int_0^H dx e^{iqx} P(x) \quad (7)$$

For convenience, we select the reference point that ensures real values of $p(q)$ at all q . For DNA, any point in the middle of the minor or major grooves can be used.

C. B-DNA helices

The *B*-form (see Fig. 2) is the most common state of DNA in aqueous solutions [37]. *B*-DNA has an inner core formed by hydrogen bonded Watson-Crick nucleotide pairs. The nucleotides are attached to two sugar-phosphate strands spiraling around the core and forming the well-known double helix that has the $H \approx 33.8 \text{ \AA}$ pitch ($g \approx 0.186 \text{ \AA}^{-1}$). Each phosphate group bears a negative charge. Their centers lie at the radial distance $a \approx 9 \text{ \AA}$ from the molecular axis. There are two phosphate groups per base pair and ≈ 10 base pairs per helical turn so that $\sigma_0 \approx 16.8 \mu\text{C}/\text{cm}^2$. The helix is fairly stiff, its persistence length is $500 \div 1000 \text{ \AA}$ (depending on the ionic strength) [see, e.g., 38 and refs. therein]. In cells and viruses, DNA is often packed within a tight compartment so that different folds of the same helix or different helices come to $\sim 5\text{-}30 \text{ \AA}$ surface-to-surface separation within each other ($R \sim 25\text{-}50 \text{ \AA}$) and form various liquid crystalline phases [4,5].

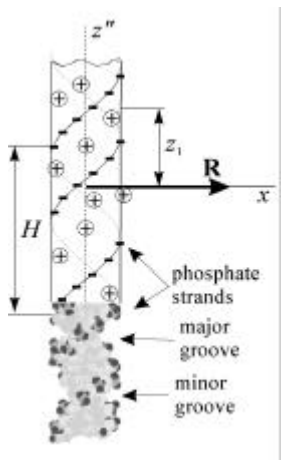


Fig. 2. Structure of *B*-DNA with negatively charged oxygens of phosphate groups shown in black (bottom) and the corresponding model of charge distribution on DNA surface (top). Adsorbed (condensed) counterions are shown schematically as residing in the major and minor grooves. The model represents molecule 1 and it is shown in the projection on (x'', z'') plane of the corresponding molecular frame (c.f. Fig. 1). \mathbf{R} is the vector connecting the points of the closest approach on the axes of molecules 1 and 2 (Fig. 1) where molecule 2 is not shown. The axial shift z_1 is the z'' coordinate of the center of the minor groove at the point where it crosses the (x'', z'') semi-plane ($x'' > 0$). The axial shift, z_2 , for the second molecule, which is not shown, is defined in the same way. [39]

Since simple structural and dimensional arguments did not explain chiral properties of liquid crystalline phases of DNA, a natural approach is to develop a statistical theory based on a chiral pair potential. Here we calculate such potential based on the simplest possible model of DNA surface charge pattern that incorporates molecular chirality. Specifically, we consider phosphate strands as continuous, charged helical lines. We distinguish four qualitatively different

types of location of adsorbed and condensed counterions: (1) on a helical line in the middle of the minor groove, (2) on a helical line in the middle of the major groove, (3) on phosphate strands, (4) random. From the corresponding model for $P(z)$, we find [26,27]

$$P(q) = \frac{1 - f_1 - f_2 - f_3}{1 - f_1 - f_2 - f_3} \left[\delta_{q,0} + f_1 \theta + f_2 \theta \cos \frac{\pi q}{g} - f_3 \theta \cos \frac{\tilde{\phi}_s q}{g} \right] \quad (8)$$

where $\delta_{x,y}$ is the Kroenecker's delta; $\tilde{\phi}_s$ ($\approx 0.4\pi$) is the azimuthal half-width of the minor groove; θ is the fraction of the charge of phosphates neutralized by adsorbed and condensed counterions; f_i are the fractions of counterions in the middle of the minor groove (f_1), in the middle of the major groove (f_2), and on the phosphate strands (f_3); $f_1 + f_2 + f_3 \leq 1$. The fraction of randomly adsorbed counterions is $1 - f_1 - f_2 - f_3$. As a reference point for $P(z)$ we select the middle of the minor groove (Fig. 2).

Of course, this model is an idealization, but at least for 150 bp DNA fragments it is quite reasonable because: (i) Such fragments are about one persistence length long (500 Å) so that they can be roughly approximated as rigid rods. (ii) As long as the energy of interaction between molecules exceeds the thermal energy ($k_B T$), thermal motions may introduce corrections, but they should not change the overall qualitative behavior of the liquid crystalline phase. (iii) For 500 Å long fragments, base pair heterogeneity does not lead to significant deviations from the ideal helix [40]. (iv) For monovalent and polymeric counterions (such as polyamines) that were used to study the cholesteric phase, discreteness of phosphate and counterion charges is not essential, e.g., the helical chain of discrete phosphates can be modeled as a continuous charged spiral [41]. (v) This model has already proved to be quite successful in several applications [26,27].

III. GENERAL RESULTS

A. Interaction at nonzero interaxial angles

In an electrolyte solution, the energy of interaction between two identical, infinitely long helices crossing at an interaxial angle $\psi \neq 0$ is given by (for detailed derivation see Appendix)

$$E_{\text{int}} \approx \frac{8\pi^3 \sigma_0^2}{\epsilon_s |\sin \psi|} \sum_{n,m=-\infty}^{\infty} \frac{\left[-1 \int^n p(-ng) p(mg) \cos [ngz_1 - mgz_2] e^{-\kappa_m R \sqrt{1+w_{n,m}^2(\psi)}} \right]}{\kappa_n \kappa_m \sqrt{1+w_{n,m}^2(\psi)} \left[1 - \tilde{\beta}_n(n) \right] \left[1 - \tilde{\beta}_m(mg) \right] K'_n(\kappa_n a) K'_m(\kappa_m a)} \times \left[\sqrt{1+w_{m,n}^2(\psi)} + w_{m,n}(\psi) \right] \left[\sqrt{1+w_{n,m}^2(\psi)} + w_{n,m}(\psi) \right] \quad (9)$$

where

$$w_{n,m}(\psi) = \frac{ng - mg \cos \psi}{\kappa_m \sin \psi}; \quad (10)$$

$$\kappa_n = \sqrt{\kappa^2 + n^2 g^2}; \quad (11)$$

$$\tilde{\beta}_n(q) = \frac{\epsilon_c}{\epsilon_s} \frac{|q|}{\kappa_n} \frac{K_n(\kappa_n a) I'_n(|q|a)}{I_n(|q|a) K'_n(\kappa_n a)}; \quad (12)$$

a is the radius of the water-impermeable molecular cores of the helices; R is the closest approach distance between molecular axes (Fig. 1); z_1 and z_2 are the axial coordinates of the helical strands relative to the points of the closest approach (see, e.g., Fig. 2); $J_m(x)$ is the Bessel function of the order m ; and $I_m(x)$, $K_m(x)$, $I'_m(x)$, and $K'_m(x)$ are the modified Bessel functions and their derivatives, respectively. The derivation of Eqs. (9)-(12) involves only one approximation, namely the truncation of the series of consecutive images after the first-order term (see Appendix). Relative contributions of higher-order images decrease as $\exp(-2(R-2a)/\lambda_D)$, where $R-2a$ is the closest approach surface separation between helices. At $R-2a > \lambda_D$, such approximation is sufficiently accurate for all practical purposes.

In further analysis of interaction between biological helices in an electrolyte solution we use that $\epsilon_c \approx 2$, $\epsilon_s \approx 80$, and $\tilde{\beta}_n \sim \epsilon_c/\epsilon_s \ll 1$. Therefore, we neglect neglect $\tilde{\beta}_n$ compared to 1. However, in a nonpolar medium $\tilde{\beta}_n \sim 1$ and it cannot be neglected.

In a nonpolar medium, after substitution of $\epsilon_c = \epsilon_s = \epsilon$ and $\kappa = 0$ into Eq. (9), we find that the energy of interaction between crossed helices is given by

$$E_{\text{int}} = \frac{8\pi^3 \sigma_0^2 a^2}{\epsilon |\sin \psi|} \sum_{n,m=-\infty}^{\infty} \frac{\int_{-1}^1 p(-ng) p(mg) \cos[ngz_1 - mgz_2] I_n(|nga|) I_m(|mga|) e^{-|mg|R\sqrt{1+\tilde{w}_{n,m}^2(\psi)}}}{|mg|\sqrt{1+\tilde{w}_{n,m}^2(\psi)}} \times \left[\int_{-1}^1 \sqrt{1+\tilde{w}_{m,n}^2(\psi)} + \tilde{w}_{m,n}(\psi) \right]^n \left[\int_{-1}^1 \sqrt{1+\tilde{w}_{n,m}^2(\psi)} + \tilde{w}_{n,m}(\psi) \right]^m, \quad (13)$$

where

$$\tilde{w}_{n,m}(\psi) = \frac{ng - mg \cos \psi}{|mg| \sin \psi}. \quad (14)$$

This is *the exact* expression for the given choice of the helical surface charge pattern.

B. Interaction between parallel helices

At $\psi \rightarrow 0$, the energy of interaction between infinitely long molecules diverges because the molecules overlap over an infinite length. In this case, the meaningful value is the energy density per unit length which can be calculated as $\lim_{L \rightarrow \infty} E_{\text{int}} / L$, where L is the length of the molecules. In other words, for infinitely long molecules, the $\psi = 0$ and $\psi \neq 0$ cases should be treated separately. A general expression for the interaction energy at $\psi = 0$ was derived in [24]. It is also recovered here in the Appendix (Eq. (A 63)). For helices with surface charge patterns given by Eq. (6), the energy density takes the form

$$\frac{E_{\text{int}}}{L} \approx \frac{8\pi^2 \sigma_0^2}{\epsilon_s} \sum_{n=-\infty}^{\infty} \int_{-1}^1 \frac{[p(n)g]^2 \cos[ng\Delta z] K_0(\kappa_n R)}{\kappa_n^2 [K'_n(\kappa_n a)]^2} , \quad (15)$$

in an electrolyte solution and

$$\frac{E_{\text{int}}}{L} = \frac{8\pi^2 \sigma_0^2 a^2}{\epsilon} \sum_{n=-\infty}^{\infty} \int_{-1}^1 [p(n)g]^2 \cos[ng\Delta z] K_0(|ng|R) I_n^2(|ng|a) \quad (16)$$

in a nonpolar medium. Here $\Delta z = z_2 - z_1$.

C. Interaction modes

Although they may seem to be cumbersome, Eqs. (9)-(16) are easy to use. Indeed, it follows from Eqs. (9),(13),(15),(16) that the total interaction energy can be represented as a sum of contributions from “interaction modes” with different indices n and m . Only a few modes with small indices give significant contributions to the total energy. The sum of modes rapidly converges because of the exponential dependence of the energy of each mode on n and m . Unless $p(n)g$ is zero or anomalously small because of a peculiar symmetry of the charge pattern, the sum can be truncated after only a few terms with $n,m \neq 0$. The truncated expressions allow us to conduct fairly detailed analysis of the interaction laws, as well as to perform rapid numerical calculation.

For instance, for homogeneously charged cylinders, $\bar{\sigma} = \sigma_0$ and $p(q) = \delta_{q,0}$. After substituting this into Eq. (9) we arrive at the classical result [17,18,42]

$$E_{\text{int}} \approx \frac{8\pi^3 \bar{\sigma}^2}{\epsilon_s \kappa^3 K_1^2(\kappa a)} \frac{e^{-\kappa R}}{|\sin \psi|} . \quad (17)$$

However, such approximation is not appropriate for helical macromolecules. It accounts for just a fraction of the net interaction energy. Most importantly, it neglects the chiral nature of helices and, therefore, chiral interactions.

For helices, the zero mode is nothing else as the contribution from the average surface charge density $\bar{\sigma}$. Chiral interactions are determined by other, “helical” modes with $n,m \neq 0$. Not only the helical modes are responsible for the chirality, but they often give a dominant contribution to the net energy. In particular, net-neutral molecules contain equal number of negatively and positively charged surface residues so that $\bar{\sigma} = 0$ while $\sigma_0 \neq 0$. Then, the interaction energy is determined exclusively by the helical modes. Molecules with high surface density of intrinsic charged residues of one sign (such as DNA) cause adsorption and/or condensation of counterions resulting in $|\bar{\sigma}| \ll |\sigma_0|$. As a result, “helical” modes may contribute much more to the interaction energy than the zero mode (at surface separations smaller than the helical pitch).

IV. INTERACTION BETWEEN INFINITELY LONG HELICES

A. Interaction between idealized *B*-DNA-like helices

First, let us illustrate the general formulae with a heuristic model of interaction between *B*-DNA-like helices. We exaggerate the rigidity, homogeneity, and length of DNA and assume that the molecules are perfect, infinitely long helices. To emphasize nontrivial features of their chiral interaction, we select a peculiar (but not impossible) surface charge pattern, i.e. $f_1=0.4$, $f_2=0.6$, $f_3=0$, and $\theta=0.8$ in Eq. (8). In Section VI, we discuss observed phenomena using a model of 150 bp DNA fragments with surface charge patterns expected to be more common.

Several energy landscapes calculated from Eq. (9) within these assumptions are shown in Fig. 3. The energy is a function of four variables: interaxial separation R , interaxial angle ψ , and axial shifts z_1 and z_2 . It is plotted at two different surface separations: one slightly larger than the Debye length is ($\lambda_D=7$ Å, $R=27$ Å, $R-2a\approx9$ Å, [43]) and the other slightly larger than $2\lambda_D$ ($R=35$ Å). Each landscape shows the energy as a function of ψ and $\Delta z=z_2-z_1$. The selected values of z_1 correspond to three most representative cases that differ in the location of the point of closest approach between the molecules with respect to strands and grooves on molecule 1. Specifically the point of the closest approach on molecule 1 is located in the center of the minor groove at $z_1=0$, on one of the phosphate strands at $z_1\approx0.2H$, and in the center of the major groove at $z_1=H/2$ (see Fig. 2).

Numerical summation of the terms in Eq. (9) confirms our expectation of rapid convergence of the sums. We find that only the modes with $n,m=0,\pm 1, \pm 2$ are important. The modes of interaction with larger indices introduce minor corrections to the energy and they can be neglected.

The energy landscapes contain deep "canyons", shallow "lakes", "ridges", "overpasses", and steep "mountains". The interaction may be energetically favorable ($E_{\text{int}}<0$) or unfavorable ($E_{\text{int}}>0$) depending on the specific alignment of the molecules and on the interaxial separation. The point of plotting all these landscapes is to demonstrate the rich variety of their features. This richness suggests that the interaction may not be reducible to simple Hamiltonians used in phenomenological models of chiral interactions.

B. Interaction at large separations

Details of the energy landscapes shown in Fig. 3 are model-specific, but the interaction also has universal features common for all helices. To gain an insight into such features, it is instructive to consider the interaction in a simple limiting case of small interaxial angles ($|\sin\psi|\ll 1$) and large surface separations ($R-2a\gg\lambda_D$). At $|\sin\psi|\ll 1$, only $n=m$ terms contribute to the sum in Eq. (9) since $w_{n,m}(\psi)|_{n\neq m}\gg 1$ and $w_{n,n}(\psi)\ll 1$. When, in addition, $\kappa(R-2a)\gg 1$ all modes except those with $n=m=0$ and $n=m=\pm 1$ can be neglected [44]. After expanding the energy at small $|\psi|$, we find

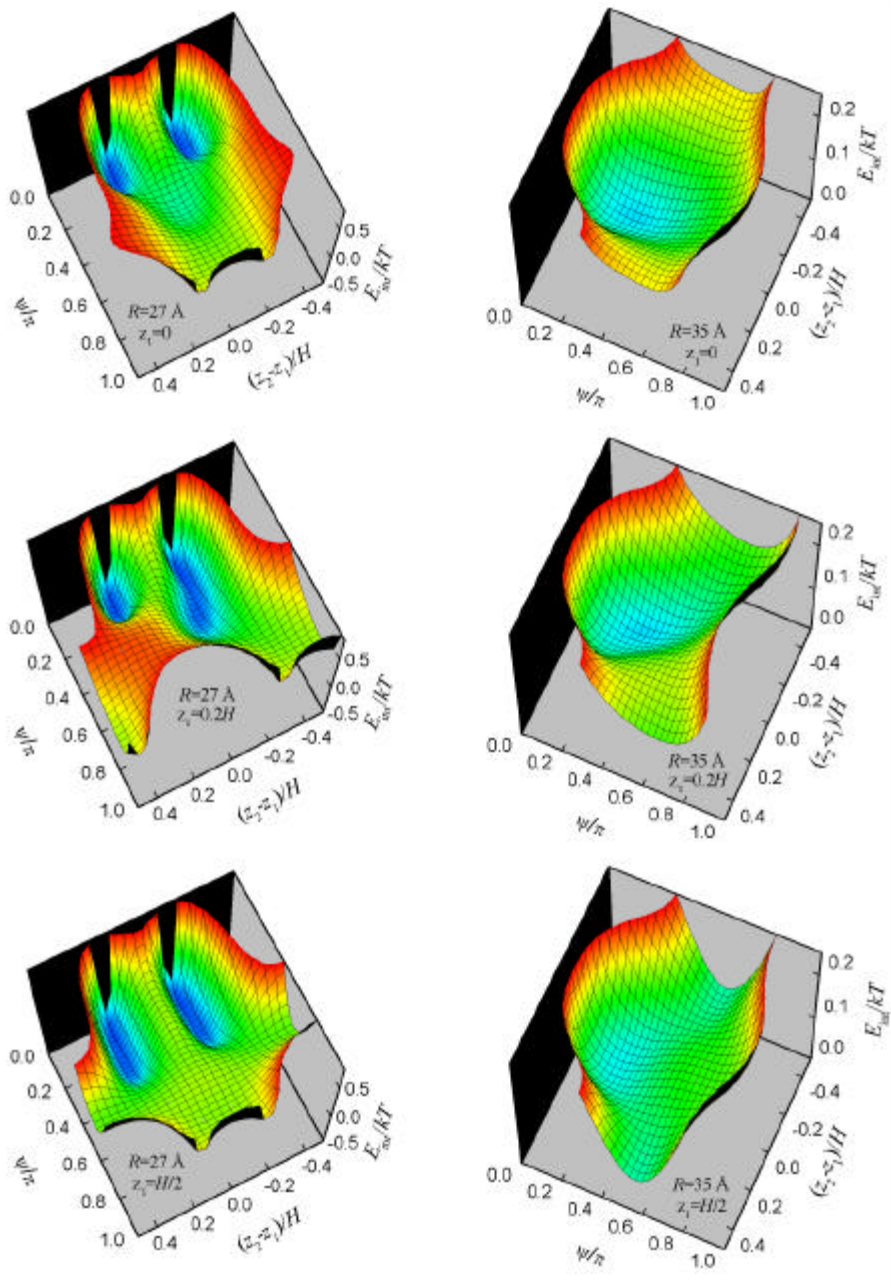


Fig. 3. Energy landscapes for interaction between two crossed *B*-DNA-like helices plotted as a function of the interaxial angle ψ and mutual axial shift z_2-z_1 for indicated values of z_1 and R . The energy is given in the units of thermal energy ($k_B T \approx 4.1 \cdot 10^{-14}$ erg ≈ 0.025 eV at $T=300$ K). For infinitely long molecules it diverges as $\sim 1/\sin\psi$ at small interaxial angles because of the increasing effective interaction length (Section V.A). For finite-length molecules, the divergence levels off. Here, it is cut off from the landscapes by limiting the energy scale. To improve visual perception, the landscapes are shown for ψ varying from 0 to π . Because of molecular symmetry, the $(z_1, -\psi)$ alignment of molecule 1 is equivalent to $(H-z_1, \pi-\psi)$, e.g., $-\psi$ is equivalent to $\pi-\psi$ at $z_1=0$ and at $z_1=H/2$.

$$\begin{aligned} \frac{\epsilon_s \kappa^3 K_1^2(\kappa a)}{8\pi^3 \sigma_0^2} E_{\text{int}} \approx & \left| \frac{\bar{\sigma}^2}{\sigma_0^2} - C \cos \psi g \Delta z \int e^{-(\kappa_1 - \kappa)R} \int e^{-\kappa R} \frac{1}{|\psi|} \right| \\ & - \frac{Cg}{\kappa_1} \cos \psi g \Delta z \int e^{-\kappa_1 R} \frac{\psi}{|\psi|} + \frac{Cg^2}{8\kappa_1^2} \cos \psi g \Delta z \int \int \kappa_1 R - 3 \int e^{-\kappa_1 R} |\psi| + \dots \end{aligned} \quad (18)$$

where $\bar{\sigma}$ is the average surface charge density [see Eq. (5)] and

$$C = 2[p(g)]^2 \frac{\kappa^3 K_1^2(\kappa a)}{\kappa_1^3 [K_1'(\kappa_1 a)]^2}. \quad (19)$$

It follows from Eq. (18) that the most energetically favorable axial alignment between the molecules is $\Delta z = 0$, regardless of the interaxial angle. At this optimal alignment, the molecular opposition may be energetically favorable ($E_{\text{int}} < 0$) or unfavorable ($E_{\text{int}} > 0$), depending on the ratio $\bar{\sigma} / \sigma_0$ and on the surface separation between molecules.

At $|\bar{\sigma}| > |\sigma_c|$, where [45]

$$\sigma_c = \sigma_0 \sqrt{C} e^{-(\kappa_1 - \kappa)a}, \quad (20)$$

the interaction is energetically unfavorable at zero and any small angle. The energy decreases with increasing interaxial angle.

When $|\bar{\sigma}| < |\sigma_c|$, the interaction is more complicated. It is energetically favorable at $R < R_c$, where

$$R_c = 2a + (\kappa_1 - \kappa)^{-1} \ln \left| \frac{\sigma_c^2}{\bar{\sigma}^2} \right|. \quad (21)$$

Within this distance range, the most favorable interaxial angle is $\psi = 0$. The molecules "recognize" each other and tend to aggregate in a conformation with parallel long axes even when both molecules have non-zero mean surface charge density. This increases the effective length of the energetically favorable molecular opposition. The attraction is due to axial charge separation. The latter allows such alignment of two helices that oppositely charged surface groups face each other, as discussed previously in the theory of interaction between parallel helices [24,27]. At $|\bar{\sigma}| \rightarrow 0$, $R_c \rightarrow \infty$.

At $R > R_c$ but $R - R_c \ll R_c$, the interaction is energetically unfavorable at parallel alignment ($\psi = 0$), but a small twist makes it favorable. The optimal angle is

$$\psi \approx \frac{2\kappa_1}{g} \sqrt{\frac{2[e^{(\kappa_1 - \kappa)(R - R_c)} - 1]}{\int \int \kappa_1 R - 3 \int}} \quad (22)$$

It increases with increasing separation. At larger R , the optimal interaxial angle goes outside of the range of the small angle approximation. The dependence of the optimal angle on R in the vicinity of R_c is shown in Fig. 4.

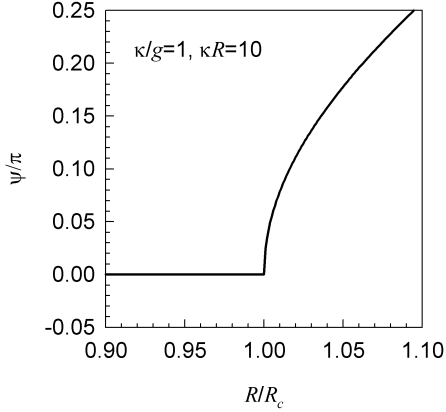


Fig. 4. The dependence of the most energetically favorable interaxial angle on interaxial separation in the asymptotic limit of large separations and small angles. The nonzero interaxial angle emerges continuously after a critical distance R_c (c.f. (22)). The value of R_c depends on the ratio between positively and negatively charges on molecular surface as described by Eq. (21). The stronger is the charge compensation, the larger is R_c .

Thus, helices tend to align parallel when they attract each other. They tend to cross at $\psi \sim \pi/2$ when they repel each other. This is something one would expect for any long, rod-like molecules. The nontrivial conclusions are the following: (a) As a result of helical surface charge pattern, two molecules can attract each other and aggregate in parallel conformation even when they have nonzero net charges of the same sign. We first described this in [24,27]. (b) The transition between $\psi=0$ and $\psi \sim \pi/2$ upon the loss of attraction occurs gradually rather than as a jump (Fig. 4). A small twist extends the range of intermolecular attraction. (c) At small interaxial angles, chirality of helices affects the direction *but not the amplitude* of the most favorable twist. Indeed, the only term in Eq. (18) that depends on the sign of ψ does not depend on the amplitude of ψ .

V. INTERACTION BETWEEN HELICES OF FINITE LENGTH

A. Effective interaction length

In real life, all helices have finite length. To understand how to apply our formalism to such helices, we use a simple argument schematically illustrated in Fig. 5. Each n -th harmonic of the surface charge density produces an electric field that decays away from the helix with the characteristic length κ_n^{-1} . The fields created by two crossed infinitely long helices overlap over the length $L_n(\psi) \sim \kappa_n^{-1} / |\sin \psi|$, as it follows immediately from the geometry of the crossed configuration. At $|\sin \psi| \ll 1$, the helices are essentially parallel in the region of their overlap. Therefore, we should be able to represent the energy of their interaction as

$$E_{\text{int}} = \sum_{n=-\infty}^{\infty} L_n \langle \psi | \mu_n | \psi \rangle \quad (23)$$

where $u_n(\psi=0)$ is the energy of interaction between parallel helices per unit of their length.

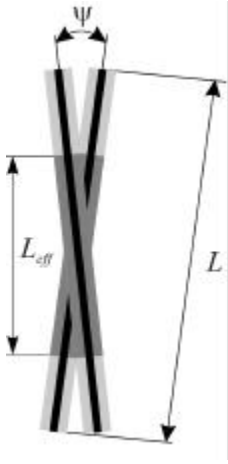


Fig. 5. Schematic illustration of interaction between two crossed, long molecules of finite length L in projection on the (y,z) plane (c.f. Fig. 1). Here the molecules are represented by solid black lines while light gray shading symbolizes electric fields around them. The region shaded in dark gray symbolizes energetically significant overlap between the electric fields. Since each n -th harmonic of the charge distribution on helical surface produces an electric field that decays exponentially away from the helix with the characteristic decay length κ_n^{-1} , the length of the overlap region for each mode is $\sim \kappa_n^{-1} / |\sin \psi|$. This is the “effective interaction length” for the mode. Only a few modes contribute significantly to the interaction. The tips of helices do not contribute much to the interaction when they protrude beyond the overlap region for all essential modes (as shown). Then, the interaction energy can be calculated assuming that the helices are infinitely long. In the opposite limit of much smaller angles, the helices are effectively parallel.

Comparing Eq. (9) with Eq. (15) we find that the expression for E_{int} at small ψ can be rewritten in the form of Eq. (23), where

$$u_n(\psi) \approx -1 \left\{ \frac{8\pi^2 \sigma_0^2 [p(ng)]^2 \cos[ng\Delta z] K_0(\kappa_n R)}{\epsilon_s \kappa_n^2 [K'_n(\kappa_n a)]^2} \times \left[1 + n^2 \frac{g \sin \psi}{\kappa_n} - (\kappa_n R + 1 - 4n^2) \frac{n^2 g^2 \sin^2 \psi}{8\kappa_n^2} + \dots \right] \right\}. \quad (24)$$

and the *effective interaction length* for each mode n is given by

$$L_n(\psi \neq 0) = \frac{\kappa_n^{-1}}{|\sin \psi|} \frac{\pi e^{-\kappa_n R}}{K_0(\kappa_n R)}. \quad (25)$$

These expressions apply also to helices of finite length if molecular tips protrude beyond the area of energetically significant overlap between the electric fields, as shown in Fig. 5. Then the contribution of the tips to the interaction energy can be neglected. Since the length of the overlap area for each mode is $L_n(\psi)$, this approximation should work when $L > L_n(\psi)$ for all essential modes. Taking into account that $L_0(\psi)$ is the largest of all L_n , we find that Eqs. (23)-(25) are applicable to helices of finite length at $|\psi| > \psi_0$, where

$$\psi_n \approx \frac{\pi}{L \kappa_n} \frac{e^{-\kappa_n R}}{K_0(\kappa_n R)} \approx \frac{\sqrt{2\pi R / \kappa_n}}{L} \quad (26)$$

is the root of equation $L_n(\psi) = L$. To obtain this expression from Eq. (25), we replaced $|\sin \psi|$ by $|\psi|$ and used the asymptotic expansion of $K_0(x)$ assuming that $\kappa R \gg 1$, which is typically the case.

Furthermore, Eqs. (23),(24) also describe the energy of interaction between parallel ($\psi=0$) helices of large finite length L ($L \gg H$) if we assume that

$$L_n(\psi=0)=L. \quad (27)$$

Two helices can be viewed as effectively parallel over their whole length when $L \ll L_n(\psi)$ for all essential modes.

Thus, we can use Eqs. (23)-(27) for finite length helices as long as $L \gg H$ and $|\psi| \ll \psi_N$ or $|\psi| \gg \psi_0$. Here N is the largest mode index that still contributes significantly to the interaction energy (e.g., $N=1$ at large separation between helices). The intermediate case of $|\psi| \sim \psi_n$ is more complicated. Its rigorous analysis requires an explicit solution for the energy of interaction between crossed helices of finite length [46]. We will discuss this case elsewhere.

B. Intermolecular torque

It was proposed that to understand the macroscopic pitch of a cholesteric phase formed by long, chiral molecules it is sufficient to know the intermolecular torque at $\psi=0$ [14,15]. This rests on the assumption that the torque is a regular, smooth function of ψ at small ψ . Let us now calculate the torque between two helices and see whether our results support such assumption.

At $\psi=0$, we find from Eqs. (23),(24), and (27) that the intermolecular torque is

$$t = -\frac{dE_{\text{int}}}{d\psi} \approx -\frac{16\pi^2\sigma_0^2}{\epsilon_s} L g \sum_{n=1}^{\infty} \left| -1 \right| \int n^2 \frac{[p(ng)]^2 \cos[ng\Delta z] K_0(\kappa_n R)}{\kappa_n^3 [K'_n(\kappa_n a)]^2}. \quad (28)$$

As we would expect, the torque changes the sign upon inversion of helical handedness ($g>0$ for right-handed and $g<0$ for left-handed helices). This torque tends to twist helices out of parallel alignment.

At $\psi_0 < |\psi| \ll 1$, we obtain from Eqs. (23)-(25)

$$t \approx \frac{\psi}{|\psi|^3} \frac{8\pi^3\sigma_0^2}{\epsilon_s} \sum_{n=-\infty}^{\infty} \left| -1 \right| \int \frac{[p(ng)]^2 \cos[ng\Delta z] e^{-\kappa_n R}}{\kappa_n^3 [K'_n(\kappa_n a)]^2} \quad (29)$$

An extrapolation of Eq. (29) to $\psi=0$ yields a diverging torque instead of Eq. (28). This means that the torque is not a smooth, regular function of ψ and that it experiences a “catastrophic” change somewhere between $\psi=0$ and $|\psi| \sim \psi_0$. If this range of ψ is important, the prediction of the cholesteric pitch based on the zero-angle torque, and the Frank free energy description of twist deformations in a cholesteric liquid crystal may fail (unless rescued by complex many-body effects). The consequences for the structure and properties of the cholesteric phase may be quite significant. We illustrate these consequences on the example of the cholesteric phase formed by “short-fragment” (~ 150 base pairs) DNA helices.

VI. ON THE ORIGIN AND STRUCTURE OF THE CHOLESTERIC PHASE FORMED BY *B*-DNA MOLECULES

As we discussed in Section II.C, the model of *B*-DNA as a rigid rod with helical surface charge distribution (Eq. (8)) should be reasonably accurate for describing electrostatic interactions between molecules whose total length is large compared to the helical pitch but smaller or equal to the persistence length. This applies to 150 bp DNA molecules whose length is ~ 500 Å and whose phase behavior was extensively studied experimentally.

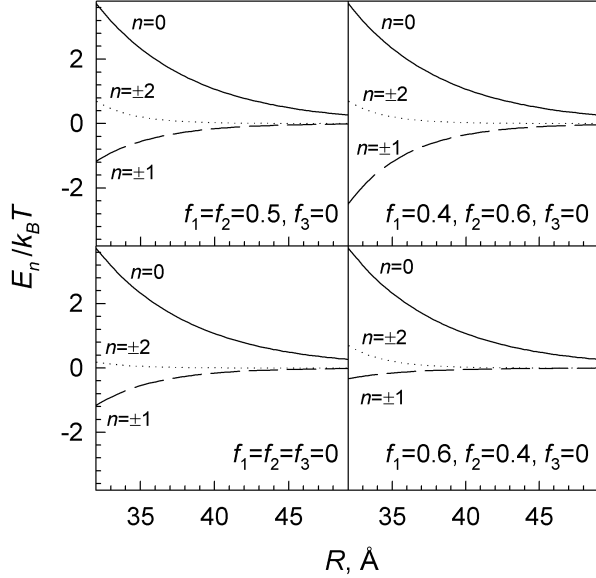


Fig. 6. Contribution of different modes to the energy of interaction between two parallel ($\psi=0$), 150 bp DNA helices at $\theta=0.75$. Each E_n is the sum of the energies of two modes with indices $\pm n$. E_n is shown in the units of thermal energy $k_B T$ (1 $k_B T \approx 4 \cdot 10^{-14}$ erg ≈ 0.025 eV at room temperature). Relative contributions of different modes to the interaction energy at small $\psi \neq 0$ are practically the same as at $\psi=0$, as follows from Eq. (24). The energy of modes with $n=\pm 3$ is not shown since it is indistinguishable from zero at the energy scale used on the graph.

In ensembles of 150 bp DNA, the cholesteric phase was observed at interaxial distances from 32 to 49 Å [2,47]. Most measurements were done in ~ 0.1 - 0.3 M NaCl or NH₄Cl ($\lambda_D \sim 5$ - 10 Å, $\theta \approx 0.75$ [48]). At these conditions, only the interaction modes with $n=m=0, \pm 1, \pm 2$ are important (see Fig. 6). From Eq. (27), we find that the corresponding ψ_n are $\psi_0 \approx 5$ deg, $\psi_{\pm 1} \approx 4$ deg, and $\psi_{\pm 2} \approx 3$ deg. The observed interaxial angle between the molecules varies from ~ 0.3 deg to 3 deg [5,6,10], exactly in the expected crossover range where the intermolecular torque rapidly changes with ψ .

Rigorous theory of the cholesteric phase, therefore, requires calculation of the potential of interaction in the crossover region and a many-body statistical theory which is beyond the scope of the present work. However, we can get a glimpse at the underlying physics from qualitative analysis of the balance between inter-molecular torques, as described in this Section. We consider an idealized cholesteric phase that consists of planar molecular layers (Fig. 7). Within each layer, the molecules are parallel. Each next layer is twisted with respect to the previous layer by a constant small angle ψ ($|\sin \psi| \ll 1$). The angle is defined to be positive for a right-handed twist and negative for a left-handed twist. We start from discussion of additivity of pair interaction potentials and other many-body effects that may be important in a multimolecular ensemble. We then proceed to analysis of torques acting between molecular layers, estimate the cholesteric

pitch, address the cholesteric-to-nematic (line-hexatic) phase transition observed upon decreasing separation between DNA helices, and discuss the sense of the twist in the cholesteric phase.

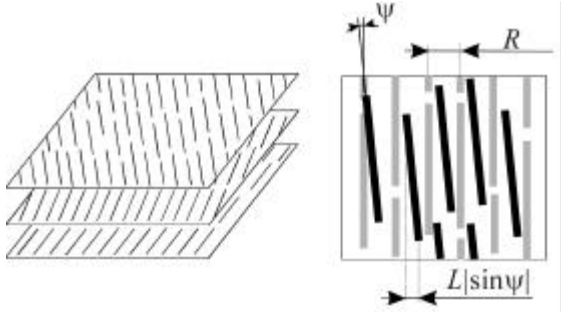


Fig. 7. *Left*. Schematic illustration of a right-handed cholesteric phase. *Right*. Mutual alignment of molecules in two neighboring layers in the cholesteric phase. Molecules in the bottom layer are shown in gray while molecules in the top layer are shown in black.

A. Pairwise additivity and many-body effects.

As we mentioned in Section II, here we consider only “frozen” surface charge patterns postponing analysis of possible effects of surface charge density fluctuations till later studies. Then, taking into account that electrostatic potentials are additive, we can find the ensemble energy by adding up energies of interaction of all pairs of DNA molecules. Furthermore, because surface separation between any two molecules in the cholesteric phase exceeds the Debye length and because the interaction energy exponentially decreases with the separation we can consider only interactions between nearest neighbors.

Despite the additivity of pair interaction potentials, the dependence of the energy on mutual alignment of molecules may introduce many-body effects. Consider, for instance, interaction between three nearest neighbor molecules that form the basic unit of local hexagonal packing (such as observed in the cholesteric phase of DNA). The energy of interaction between each two of the molecules v, μ ($=1,2,3$) depends on their mutual axial alignment $\Delta z_{v,\mu}$ (see Eq. (24)). The many body effects are due to the relationship between $\Delta z_{v,\mu}$ that has the form

$$\Delta z_{1,3} = \Delta z_{1,2} - \Delta z_{2,3}. \quad (30)$$

In principle, a twist between molecular layers may lead to even more complex many-body effects if a molecule in one layer crosses with more than one molecule in a neighboring layer. However, this is not the case in the cholesteric phase of *B*-DNA. Indeed, in projection on the neighboring layer, a molecule traverses the distance $L|\sin \psi|$ in the direction normal to molecules of the layer (Fig. 7). At the interaxial angles characteristic for the cholesteric phase $\psi \leq 3$ deg, this distance does not exceed 25 Å, i.e. it is always smaller than the interaxial distance ($R > 32$ Å) between molecules.

B. Force balance and cholesteric pitch

Consider the balance of torques between molecular layers. As we found in Section V, it is convenient to analyze the regions of $|\psi| \ll \psi_2$ and $\psi > \psi_1$ separately.

$|\mathbf{y}| \ll \mathbf{y}_2$: At such small angles the molecules are effectively parallel (see Section V). Their interaction energy is determined primarily by the mode with $n=0$, but this mode does not

contribute to intermolecular torque. The torque is determined by the modes with $n \neq 0$. After substitution of Eq. (8) into Eq. (28), we find that the average torque between neighboring layers (normalized per one molecule) is

$$\langle t \rangle \approx \frac{8\pi^2 \sqrt{6\pi} L g \sigma_0^2 e^{-\kappa_1 R}}{\varepsilon_s \kappa_1^3 \sqrt{\kappa_1 R} [K'_1(\kappa_1 a)]^2} \left[\langle \cos[g\Delta z_{v,\mu}] \rangle [f_2 - f_1] \theta + \cos[\tilde{\phi}_s] \right]^2 - 4 \langle \cos[2g\Delta z_{v,\mu}] \rangle [f_2 + f_1] \theta - \cos[2\tilde{\phi}_s] \right]^2 \frac{\kappa_1^{7/2} [K'_1(\kappa_1 a)]^2}{\kappa_2^{7/2} [K'_2(\kappa_2 a)]^2} e^{-\kappa_2 - \kappa_1 \theta R} \quad (31)$$

Here $\langle \rangle$ indicates averaging over axial shifts $\Delta z_{v,\mu}$ between nearest neighbor molecules v and μ (see previous Section). We assume that all counterions are located in the grooves, i.e. $f_3 = 0$, since counterion adsorption on the phosphate strands simply renormalizes the phosphate charge (the value of σ_0). Taking into account that $\kappa_n R \gg 1$, we use the asymptotic expansion of $K_0(\kappa_n R)$. The first term in Eq. (31) is the contribution of $n = \pm 1$ modes. At $f_2 - f_1 = \cos[\tilde{\phi}_s] \theta \approx 0.43$, it vanishes so that we must also include the second term that describes the contribution of $n = \pm 2$ modes. The contribution of modes with larger $|n|$ is negligible.

This torque is chiral, it tends to establish either right-handed or left-handed twist between molecular layers depending on the handedness of DNA helices, average $\Delta z_{v,\mu}$, and on the partition of counterions between the major and minor grooves. This torque is the driving force for formation of the cholesteric phase.

$|\psi| > \psi_1$: In this case, the chiral contribution of $n = \pm 1, \pm 2$ modes to the torque is negligible compared to non-chiral contribution of the same modes ($n = \pm 1, \pm 2$ terms in Eq. (29)). Therefore, the net torque is predominantly non-chiral. From symmetry, a non-chiral torque can favor only parallel conformation of the layers. In other words, regardless of which mode contributes the most ($n = 0$, $n = \pm 1$, or $n = \pm 2$), the net torque tends to reduce the twist between the layers. As a result, $|\psi| > \psi_1$ is always energetically unfavorable.

Thus, the net torque is chiral and it tends to twist helices out of parallel alignment at $|\psi| < \psi_2$. The situation reverses at $|\psi| > \psi_1$. The predominantly non-chiral net torque tends to twist helices back to the parallel alignment. The competition between these torques may produce a nonzero equilibrium interaxial angle $|\psi_{eq}| < \psi_1$.

The pitch of the cholesteric phase (P) is related to $|\psi_{eq}|$ as $P = \sqrt{3}\pi R / |\psi_{eq}|$ [49]. Since $|\psi_{eq}| < \psi_1$, the pitch of the cholesteric phase should be larger than $P_{min} = \sqrt{3}\pi R_{min} / \psi_1$, where R_{min} is the smallest interaxial separation between helices in the cholesteric phase. After substituting Eq. (26), we find

$$P_{min} \approx \sqrt{3} \pi L \left[\left(\frac{R_{min}}{H} \right)^2 + \left(\frac{R_{min}}{2\pi\lambda_D} \right)^2 \right]^{1/4} \quad (32)$$

Using $R_{\min} \approx 32 \text{ \AA}$ [47], $H \approx 34 \text{ \AA}$, $L \approx 500 \text{ \AA}$, and $\lambda_D \approx 5-10 \text{ \AA}$, we obtain $P_{\min} \approx 0.3 \mu\text{m}$. This allows us to understand why the cholesteric pitch is many orders of magnitude larger than typical interaxial distances between DNA. Our prediction is in good agreement with experiments. Indeed, the smallest pitch observed for 150 bp DNA is $\sim 0.2-0.4 \mu\text{m}$ [6].

C. Cholesteric-to-nematic phase transition

It follows from Eq. (31) that the average chiral torque has a nonzero value only when axial alignment between molecules is not random, i.e. $\langle \cos[g\Delta z_{v,\mu}] \rangle \neq 0$ and/or $\langle \cos[2g\Delta z_{v,\mu}] \rangle \neq 0$.

This can be easily understood by taking into account that an axial shift Δz of a helical molecule with the pitch H is equivalent to rotation of the molecule around its central axis by $2\pi\Delta z/H$. Random axial alignment corresponds to random rotation. At random rotation, the molecular symmetry and intermolecular interactions become effectively uniaxial [14,50]. It is well known that the chiral cholesteric phase can not be formed as a result of non-chiral, uniaxial interactions [15,51]. Therefore, correlations in axial alignment of helices play critical role in the cholesteric phase formation.

The strength and range of axial correlations depends on the optimal (most energetically favorable) value of pairwise $\Delta z_{v,\mu}$. Indeed, from Eq. (30) we find that only $\Delta z=0$ and $\Delta z=\pm H/3$ can be simultaneously optimal for all pairs of molecules in an aggregate with local hexagonal symmetry, such as the cholesteric phase of DNA. By minimizing the energy given by Eqs. (23), (24) with respect to Δz and taking into account only the modes with $|n| \leq 2$, we find that $\Delta z=\pm H/3$ is always energetically unfavorable while $\Delta z=0$ is optimal at $R \geq R_*$, where

$$R_* \approx \frac{1}{\kappa_2 - \kappa_1} \ln \left\{ \frac{4 \left[\left| f_2 + f_1 \left(\theta - \cos[2\tilde{\phi}_s] \right) \right|^2 \left[K'_1(\kappa_1 a) \right]^2 \kappa_1^{5/2} \right]}{\left[\left| f_2 - f_1 \left(\theta + \cos[2\tilde{\phi}_s] \right) \right|^2 \left[K'_2(\kappa_2 a) \right]^2 \kappa_2^{5/2} \right]} \right\} \quad (33)$$

At $R < R_*$, the optimal value of Δz gradually increases with decreasing R . However, $\Delta z=0$ remains more energetically favorable than completely random alignment as long as $R \geq R'_*$, where

$$R'_* \approx R_* - \frac{\ln 40}{\kappa_2 - \kappa_1} \quad (34)$$

Nonzero value of $\Delta z_{v,\mu}$ results in non-optimal alignment of at least some pairs of nearest neighbor molecules causing a frustration of axial correlations. We expect this frustration to reduce the range of axial correlations to several nearest neighbors only. If this is true, the average chiral torque between macroscopic layers of molecules is zero at $\Delta z_{v,\mu} \neq 0$. Then, the cholesteric arrangement of molecules should be replaced by nematic or columnar. Since $\Delta z_{v,\mu}=0$ becomes non-optimal at $R < R_*$ and energetically unfavorable (with respect to random alignment) at $R < R'_*$, the cholesteric-to-nematic transition should occur somewhere between R'_* and R_* upon decreasing intermolecular distance. The values of R'_* and R_* depend on the partitioning of

counterions between major and minor grooves of DNA as illustrated in Fig. 8a. In particular, at $f_1=f_2=0.5$ and $\lambda_D \approx 7 \text{ \AA}$ we find $R_*' \approx 29 \text{ \AA}$ and $R_* \approx 37 \text{ \AA}$. This is in good agreement with the experimental observation that the cholesteric-to-nematic transition occurs at $R \approx 32 \text{ \AA}$ [47].

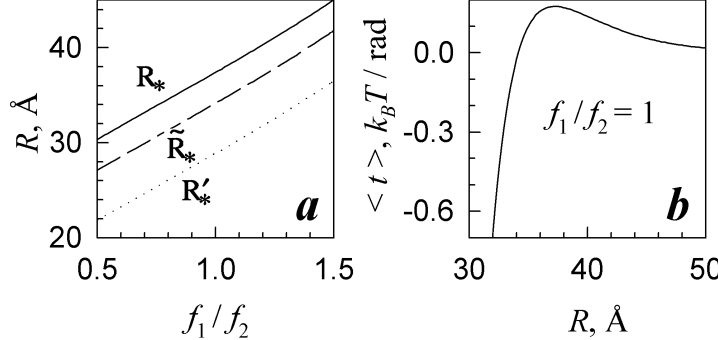


Fig. 8. Chiral torque between neighboring molecular layers in the cholesteric phase of 150 bp DNA at $|\psi| \ll \psi_2$ (3 deg) and $\Delta z_{v,\mu} = 0$. (a) Dependence of R_* , R'_* , and \tilde{R}_* on the ratio of ions in the minor and major grooves (f_1/f_2). At $R < R_*$, the axial alignment with $\Delta z = 0$ becomes non-optimal for each pair of molecules (but it still may remain optimal for a cholesteric aggregate because of many-body interactions). At $R < R'_*$, the axial alignment with $\Delta z = 0$ becomes energetically unfavorable compared to random alignment. At $R = \tilde{R}_*$, the average torque changes its sign. (b) Dependence of the average torque (normalized per one molecule) on interaxial distance at $f_1/f_2 = 1$.

Of course, this model is only a rough qualitative approximation. Still, it suggests that the physics of the transition may be in the loss of “long-range” axial helix-helix correlations with decreasing interaxial distance. This mechanism is supported by recent experimental work suggesting that the nematic phase of DNA at $R < 32 \text{ \AA}$ is not twisted and that it has a hexatic order in lateral direction [12,52]. The absence of a twist is an indication of uniaxial interactions. It was explained by the authors of Ref. [12] in exactly the same terms of frustration of pair molecular alignments based on optimal $\Delta z \neq 0$ predicted in our earlier work [24] for parallel helices.

D. Cholesteric twist inversion

It follows from Eq. (31) that the sign of the torque between molecular layers in the cholesteric phase depends on the handedness of helices (sign of g). However, the direction of the torque may change even when the helical handedness remains the same. The other factors affecting it are axial correlations between molecules and interaxial separation. To illustrate this, consider a heuristic model where we assume that macroscopic cholesteric arrangement of DNA may exist only at $\Delta z = 0$ [53].

Within this model, we find that the torque between molecular layers has a positive sign (favoring right-handed cholesteric twist) at $R \geq \tilde{R}_*$ and a negative sign (favoring left-handed cholesteric twist) at $R < \tilde{R}_*$, where

$$\tilde{R}_* \approx R_* - \frac{\ln \left| \kappa_2 / \kappa_1 \right|}{\kappa_2 - \kappa_1}. \quad (35)$$

We find that $R'_* < \tilde{R}_* < R_*$ because $\ln \left| \kappa_2 / \kappa_1 \right| = 0.5 \ln \left[(\kappa^2 + 4g^2) / (\kappa^2 + g^2) \right] < \ln(4)$. The dependence of \tilde{R}_* on partitioning of ions between minor and major grooves of DNA is shown in Fig. 8a. Thus, if the cholesteric-to-nematic transition occurs at $R < \tilde{R}_*$, the cholesteric phase may have a right-handed twist at $R > \tilde{R}_*$ and a left-handed twist at $R < \tilde{R}_*$ (Fig. 8b). If the transition occurs at $R > \tilde{R}_*$, the cholesteric phase should be always right-handed.

The origin of the right-handed twist is intuitively clear, as illustrated in Fig. 9. Right-handed rotation of molecular axes reduces the angle between opposing phosphate strands. It allows strands to face grooves on the opposing molecule. This should be energetically favorable for electrostatic and steric reasons. However, our intuition fails at $R < \tilde{R}_*$ where the inversion of the twist direction may occur. This is a manifestation of the complex, double-stranded character of DNA surface charge pattern.

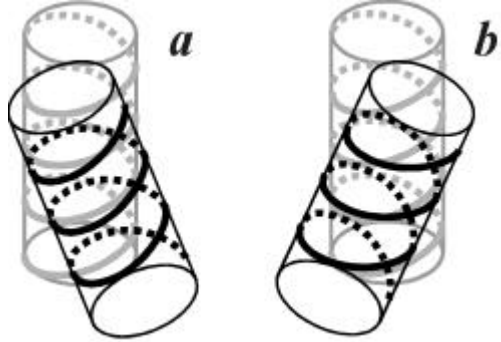


Fig. 9. Molecular alignment at right-handed (a) and left-handed (b) cholesteric twist. Front molecule is painted black while back molecule is painted gray. Note that right-handed twist allows the front molecule to fit its helical strands in the middle of the groove on the opposing surface. In contrast, left-handed twist results in strands crossing each other. Intuitively, for single-stranded, right-handed helices (such as shown) the right-handed cholesteric twist should be more energetically favorable both for electrostatic and steric reasons. One may expect this trend to be preserved for double-stranded helices such as DNA, but the geometry of interaction between double-stranded helices is more complicated. As a result, an inversion of the torque direction becomes possible.

Experimentally, the direction (sense) of the twist in cholesteric aggregates formed by polymer and salt induced DNA precipitation was studied by measurement of circular dichroism (CD) spectra in the absorption band of DNA base pairs (~260 nm) [54]. Anomalously strong, negative CD spectra measured in these experiments were interpreted as resulting from left-handed cholesteric twist of DNA. It was presumed that strong, negative CD is observed in the direction of the cholesteric twist axis and that it is related to the twist sense.

Such interpretation is, however, questionable. Specifically, a characteristic peak in CD intensity was observed within the absorption band at ~ 260 nm [54]. Such dichroism is due to electronic transitions caused by interaction of the electric vector of light with the conjugated π electron system of DNA bases rather than due to light scattering. The corresponding transition dipoles lie in the plane of DNA bases. This plane is normal to the axis of B-DNA [37] and, therefore it is parallel to the cholesteric twist axis and, correspondingly, to the direction in which the anomalous CD signal is supposed to be observed. Under such conditions, one component of the electric vector of circularly polarized light is parallel to transition dipoles. The second component is normal to transition dipoles and it cannot cause electronic transitions. In this idealized geometry, only the first component of light polarization would be absorbed. In other

words, ideal *B*-DNA packed into an ideal cholesteric phase should not be able to distinguish left from right circularly polarized light in the direction of the cholesteric twist axis. Of course, in a real cholesteric phase composed of real *B*-DNA molecules, the plane of transition dipoles may not be perfectly parallel to the cholesteric twist axis so that some circular dichroism may be observed in this direction. However, the corresponding CD signal in the absorption band should be small rather than anomalously large.

The danger of deducing the cholesteric twist sense from optical activity of aggregates in the absorption band is further emphasized by the following. The observed optical rotary dispersion of xanthan was interpreted as originating from left-handed cholesteric twist of aggregates formed by this double-stranded, charged polysaccharide [55]. However, a more direct optical method based on scattering of circularly polarized light at the wavelength that matches the cholesteric pitch revealed that the cholesteric phase of xanthan is right-handed rather than left-handed [1]. (The right-handed cholesteric phase should reject (backscatter) the right-polarized light and let the left-polarized light through [51].) The twist sense in xanthan is more in line with intuitive expectations and with our analysis showing that the right-handed cholesteric phase should be more common for right-handed helices.

If it does exist, the left-handed cholesteric twist of DNA can be explained by the cholesteric twist inversion at $R < \tilde{R}_*$. Such explanation could be verified by measurement of the dependence of the twist direction on the distance between DNA helices. However, to the best of our knowledge, such measurements were never done. As a circumstantial evidence of possible cholesteric twist inversion, we can only cite that such phenomenon was observed for aggregates of poly- γ -benzyl-glutamate α -helices upon changing solvent composition in dioxane/methylene chloride mixtures [7].

In other words, in the absence of direct experimental data confirming or refuting the left-handed arrangement, the question of the sense of the cholesteric twist in DNA aggregates and of the possibility of its inversion remains open.

VII. CONCLUSIONS

In summary, our ultimate goal is a theory of chiral liquid crystalline phases based on microscopic, chiral potentials of interaction between helical macromolecules. The present work is a step toward achieving it. In the Appendix, we report a mathematical formalism for electrostatic interaction between macromolecules with rod-like cores and arbitrary (but fixed) surface charge patterns at all interaxial angles. In the main text, we discuss the application of this formalism to helical macromolecules. We illustrate how it can be used for qualitative estimates and for explaining several puzzling features of the cholesteric phase of DNA. In our opinion, some of the most nontrivial conclusions (that reveal the complex physics of chiral electrostatic interaction between helical macromolecules) are the following:

- (i) The chiral contribution to the energy of interaction between two infinitely long molecules depends on the interaxial angle ψ as $\sin\psi/|\sin\psi|$ at $|\sin\psi| \ll 1$. *The chiral interaction determines the direction but not the amplitude of the most favorable twist.* The associated intermolecular torque depends on ψ as $\delta(\psi)$, i.e. it becomes important only at extremely small angles.
- (ii) The energy of chiral interaction between two helices of finite (large) length reveals that *the molecular length plays a critical role in the balance between chiral and nonchiral torques*

and in setting the equilibrium interaxial angle between helices. The intermolecular torque is chiral, large, and independent of ψ when the molecules are long but ψ is so small that the molecular tips are close together and the molecules are effectively parallel. The torque becomes essentially nonchiral when ψ is still small, but molecular tips are sufficiently separated so that they do not contribute to the interaction any more (Fig. 5). The balance of chiral and nonchiral torques determines the equilibrium interaxial angle between the molecules.

(iii) *The equilibrium interaxial angle is “anomalously” small and the cholesteric pitch is macroscopic in aggregates of helical macromolecules because of the large molecular length (L).* For instance, the expected pitch (P) of the cholesteric phase formed by 150 base pair *B*-DNA molecules is larger than 0.3 μm ($P > \sqrt{3} \pi L \sqrt{R/H} \sim \sqrt{3} \pi L$, $L \approx 500 \text{ \AA}$, $R = 32\text{--}49 \text{ \AA}$ is the interaxial separation between molecules, and $H \approx 34 \text{ \AA}$ is the molecular pitch). This is in good agreement with experimental observations [5,6,10].

(iv) The average torque between layers of parallel molecules is chiral only when the axial alignment between helical strands on opposing molecules exhibits long range correlations. *The cholesteric-to-nematic transition seems to be related to frustration of this alignment that occurs upon decreasing separation between DNA helices.* The predicted range of separations for the frustration onset is in good agreement with observed separations at the cholesteric-to-nematic transition [47].

(v) *The sense of the cholesteric twist is determined not only by the handedness of molecules in the aggregate, but also by counterion adsorption pattern and by interaxial separation between helices.* An inversion of the cholesteric twist of DNA from right-handed at large separations to left-handed at small separations is possible. Such inversion may explain the left-handed twist in DNA aggregates suggested based on observation of anomalously strong, negative circular dichroism spectra from polymer and salt induced DNA aggregates [54] (if the reported interpretation of these spectra is correct).

The agreement between the estimates and experimental observations suggests that we may be on the right way. However, a rigorous statistical theory of chiral aggregates of helical macromolecules, based on the pair potentials obtained in this paper, is still to be worked out.

Acknowledgments

The authors are thankful to Yu. Evdokimov, P. Hansen, A. Khokhlov, A. Liu, A. Parsegian, R. Podgornik, and D. Rau for useful discussions. A part of this work was performed within the 1998 summer-fall program on “Electrostatic Effects in Complex Fluids and Biophysics” at the Institute for Theoretical Physics, University of California at Santa Barbara (ITP). We are thankful to the program organizers: W. Gelbart, A. Parsegian, and P. Pincus - for the invitation to this program, the ITP staff for hospitality, and acknowledge the National Science Foundation, Grant No. PHY94-07194 which made our participation possible. AAK also appreciates the financial support of his regular visits to Bethesda by the National Institute of Child Health and Human Development, NIH which allowed to accomplish this project.

Appendix

CALCULATION OF PAIR INTERACTION POTENTIAL

1. OUTLINE

Consider interaction between two infinitely long, rigid molecules with arbitrary surface charge patterns. The molecules may cross at an arbitrary angle ψ . The distance of closest approach between their axes is R . The molecules have cylindrical inner cores with the same radius a . The molecular cores do not intersect ($R>2a$). We assume that fixed surface charges, adsorbed ions, and condensed counterions lie at the core/water interface (see Section II A). The molecular configuration and the coordinate systems we use to describe it are shown in Fig. 1.

We describe all charges at each core/water interface explicitly by the charge densities $\rho_v(\mathbf{r})$ defined in Cartesian coordinates of the "laboratory" frame whose z -axis coincides with the long axis of molecule 2 (Fig. 1). To calculate the electric field outside inner molecular cores, we use the standard method of induced surface charges.

Specifically, the Fourier transform of the electrostatic potential $\varphi(\mathbf{r})$ is given by

$$\tilde{\varphi}(\mathbf{k}) = \sum_{v=1}^2 G(k) [\tilde{\rho}_v(\mathbf{k}) + \tilde{\rho}_v^{ind}(\mathbf{k})]. \quad (\text{A } 1)$$

Here $\tilde{\rho}_v(\mathbf{k})$ and $\tilde{\rho}_v^{ind}(\mathbf{k})$ are the Fourier transforms of $\rho_v(\mathbf{r})$ and of the induced charge density, respectively.

$$G(k) = \frac{4\pi}{\epsilon_s [k^2 + \kappa^2]} \quad (\text{A } 2)$$

is the electrostatic Green's function in the \mathbf{k} -space, $k=|\mathbf{k}|$, $\kappa^{-1}=\lambda_D$ is the Debye length, and ϵ_s is the solvent (water) dielectric constant. The Fourier transform of any function $f(\mathbf{r})$ is defined as follows

$$\tilde{f}(\mathbf{k}) = \frac{1}{(2\pi)^{3/2}} \int d^3\mathbf{r} f(\mathbf{r}) e^{i\mathbf{kr}} \quad \text{and} \quad f(\mathbf{r}) = \frac{1}{(2\pi)^{3/2}} \int d^3\mathbf{k} \tilde{f}(\mathbf{k}) e^{-i\mathbf{kr}}, \quad (\text{A } 3)$$

Because of the cylindrical shape of inner molecular cores, it is convenient to describe the surface charge densities in two separate "molecular" frames in cylindrical coordinate systems (z, ϕ, r) , each associated with the corresponding molecular axis (see Fig. 1),

$$\rho_v(\mathbf{r}) = \rho_v(z, \phi, r) = \sigma_v(z, \phi) \delta(r - a) \quad (\text{A } 4)$$

In the first order approximation, we truncate the summation of consecutive images after the leading term. Then, the electrostatic interaction energy is given by,

$$E_{\text{int}} \approx \int d^3\mathbf{k} [\tilde{\rho}_1(\mathbf{k}) + \tilde{\rho}_{1,0}^{\text{ind}}(\mathbf{k})] \tilde{\rho}_2(-\mathbf{k}) + \tilde{\rho}_{2,0}^{\text{ind}}(-\mathbf{k})] G(k). \quad (\text{A 5})$$

where $\tilde{\rho}_{v,0}^{\text{ind}}(\mathbf{k})$ is the density of the induced charge on the surface of the core of the molecule v in the absence of the second molecule. This approximation is appropriate when the surface separation between molecules is larger than the Debye length.

By recalculating $\tilde{\rho}_v(\mathbf{k})$ and $\tilde{\rho}_{v,0}^{\text{ind}}(\mathbf{k})$ from $\tilde{\sigma}_v(q, n)$ we find an expression for the interaction energy in terms of $\tilde{\sigma}_v(q, n)$. This expression involves nontrivial integrals because one of the cylindrical coordinate systems is rotated with respect to the Cartesian laboratory frame. Nevertheless, for helical surface charge patterns these integrals can be calculated exactly yielding an analytical expression for the interaction energy which is the main result of the present work.

2. FOURIER TRANSFORMS OF CHARGE DENSITY

Molecule “2”

The long axis of this molecule coincides with z axis of the chosen Cartesian “laboratory frame” (Fig. 1). We can therefore use the expression derived in our previous work²⁴

$$\tilde{\rho}_2(\mathbf{k}) + \tilde{\rho}_2^{\text{ind}}(\mathbf{k}) = \frac{a}{(2\pi)^{1/2}} \sum_{m=-\infty}^{\infty} i^m [\tilde{\sigma}_2(q, m) + \tilde{\sigma}_2^{\text{ind}}(q, m)] J_m(Ka) e^{-im\phi_{\mathbf{k}}} \quad (\text{A 6})$$

This expression converts the Fourier transforms of the charge density from cylindrical coordinates (coaxial with the main axis of the molecule) into the Cartesian coordinates, $\mathbf{k}=(q, K, \phi_{\mathbf{k}})$.

While we treat the surface density of fixed and adsorbed charges, $\tilde{\sigma}_2(q, m)$, as known, the density of induced charges, $\tilde{\sigma}_2^{\text{ind}}(q, m)$, is to be calculated. When the molecules are not too close to each other, the series of consecutive images rapidly converges. In the first order approximation, we may replace $\tilde{\sigma}_2^{\text{ind}}(q, m)$ by $\tilde{\sigma}_{2,0}^{\text{ind}}(q, m)$ which is the surface density of induced charges in the absence of molecule 1. To calculate $\tilde{\sigma}_{2,0}^{\text{ind}}(q, m)$, we first find the electrostatic potential created by σ_2 and $\sigma_{2,0}^{\text{ind}}$, as if $\sigma_{2,0}^{\text{ind}}$ were known. Then, we use the continuity of the potential and of the normal component of electric induction at the inner-core/water interface to find $\sigma_{2,0}^{\text{ind}}$.

The electrostatic potential created by molecule 2 in the absence of molecule 1 is

$$\tilde{\Phi}_2(\mathbf{k}) + \tilde{\Phi}_{2,0}^{\text{ind}}(\mathbf{k}) = \frac{2a(2\pi)^{1/2}}{\epsilon_s [k^2 + \kappa^2]} \sum_{m=-\infty}^{\infty} i^m [\tilde{\sigma}_2(q, m) + \tilde{\sigma}_{2,0}^{\text{ind}}(q, m)] J_m(Ka) e^{-im\phi_{\mathbf{k}}} \quad (\text{A 7})$$

In cylindrical coordinates:

$$\begin{aligned} \varphi_2(z, \phi, r) + \varphi_{2,0}^{ind}(z, \phi, r) &= \frac{a}{\pi \epsilon_s} \int_{-\infty}^{\infty} dq \int_0^{\infty} K dK \int_0^{2\pi} d\phi_K \frac{e^{-iqz} e^{-iKrcos(\phi_K - \phi_r)}}{[q^2 + K^2 + \kappa^2]} \\ &\quad \sum_{m=-\infty}^{\infty} i^m [\tilde{\sigma}_2(q, m) + \tilde{\sigma}_{2,0}^{ind}(q, m)] J_m(Ka) e^{-im\phi_K} \end{aligned} \quad (\text{A 8})$$

The integration over ϕ_K gives

$$\tilde{\varphi}_2(q, m, r) + \tilde{\varphi}_{2,0}^{ind}(q, m, r) = \frac{4\pi a}{\epsilon_s} [\tilde{\sigma}_2(q, m) + \tilde{\sigma}_{2,0}^{ind}(q, m)] \int_0^{\infty} K dK \frac{J_m(Ka) J_m(Kr)}{[q^2 + K^2 + \kappa^2]} \quad (\text{A 9})$$

Note that fixed and adsorbed charges are located at $r=a+0$ while induced charges are located at $r=a-0$. The potential inside this infinitesimally thin layer ($a-0 < r < a+0$) is given by

$$\tilde{\varphi}_2(q, m, r) + \tilde{\varphi}_{2,0}^{ind}(q, m, r) = \frac{4\pi a}{\epsilon_s} [\tilde{\sigma}_2(q, m) K_m(\tilde{\kappa}_q a) I_m(\tilde{\kappa}_q r) + \tilde{\sigma}_{2,0}^{ind}(q, m) I_m(\tilde{\kappa}_q a) K_m(\tilde{\kappa}_q r)] \quad (\text{A 10})$$

where

$$\tilde{\kappa}_q = \sqrt{\kappa^2 + q^2} \quad (\text{A 11})$$

The potential inside the molecular core is a solution of the Poisson equation whose general form is

$$\tilde{\varphi}_2^{core}(q, m, r) = B(q, m) I_m(|q|r) \quad (\text{A 12})$$

where $B(q, m)$ is an integration constant. From continuity of the potential at the core we find

$$B(q, m) = \frac{4\pi a}{\epsilon_s} [\tilde{\sigma}_2(q, m) + \tilde{\sigma}_{2,0}^{ind}(q, m)] K_m(\tilde{\kappa}_q a) \frac{I_m(\tilde{\kappa}_q a)}{I_m(|q|a)} \quad (\text{A 13})$$

and

$$\tilde{\varphi}_2^{core}(q, m, r) = \frac{4\pi a}{\epsilon_s} [\tilde{\sigma}_2(q, m) + \tilde{\sigma}_{2,0}^{ind}(q, m)] K_m(\tilde{\kappa}_q a) \frac{I_m(\tilde{\kappa}_q a)}{I_m(|q|a)} I_m(|q|r) \quad (\text{A 14})$$

The continuity of the normal component of electric induction gives

$$\left. \frac{\partial [\tilde{\varphi}_2(q, m, r) + \tilde{\varphi}_{2,0}^{ind}(q, m, r)]}{\partial r} \right|_{r=a} = \frac{\epsilon_c}{\epsilon_s} \left. \frac{\partial \tilde{\varphi}_2^{core}(q, m, r)}{\partial r} \right|_{r=a}, \quad (\text{A 15})$$

where ϵ_c and ϵ_s are the dielectric constants inside and outside of molecular cores, respectively. After substituting Eqs. (A 10), (A 14) into Eq. (A 15) we obtain [56]

$$[\tilde{\sigma}_2(q, m) + \tilde{\sigma}_{2,0}^{ind}(q, m)] = -\frac{\tilde{\sigma}_2(q, m)}{\tilde{\kappa}_q a [1 - \tilde{\beta}_m(q)] I_m(\tilde{\kappa}_q a) K'_m(\tilde{\kappa}_q a)} \quad (A 16)$$

where

$$\tilde{\beta}_m(q) = \frac{\epsilon_c}{\epsilon_s} \frac{|q|}{\tilde{\kappa}_q} \frac{K_m(\tilde{\kappa}_q a) I'_m(|q|a)}{I_m(|q|a) K'_m(\tilde{\kappa}_q a)} \quad (A 17)$$

Finally, after substitution of Eq. (A 17) into Eq. (A 6), we arrive at

$$\tilde{\rho}_2(\mathbf{k}) + \tilde{\rho}_{2,0}^{ind}(\mathbf{k}) = -\frac{1}{(2\pi)^{1/2}} \sum_{m=-\infty}^{\infty} i^m \frac{\tilde{\sigma}_2(q, m) J_m(Ka) e^{-im\phi_{\mathbf{k}}}}{\tilde{\kappa}_q [1 - \tilde{\beta}_m(q)] I_m(\tilde{\kappa}_q a) K'_m(\tilde{\kappa}_q a)} \quad (A 18)$$

Molecule “1”

The calculation of $\tilde{\rho}_1(\mathbf{k}) + \tilde{\rho}_{1,0}^{ind}(\mathbf{k})$ is more involved because molecule 1 is shifted and rotated with respect to the z -axis of our Cartesian laboratory frame. Thus, we introduce two auxiliary Cartesian coordinate systems as follows (Fig. 1):

- $\mathbf{r}' \equiv (x', y', z')$ is shifted from (x, y, z) by the vector $-\mathbf{R}$ connecting the points of the closest approach of the axes of molecules 1 and 2;
- $\mathbf{r}'' \equiv (x'', y'', z'')$ is obtained by rotation of (x', y', z') by the angle ψ so that z'' coincides with the axis of molecule 1.

We use ρ' and ρ'' to denote the charge density function in (x', y', z') and (x'', y'', z'') coordinates correspondingly.

Since

$$\rho_1(\mathbf{r}) + \rho_{1,0}^{ind}(\mathbf{r}) = \rho'_1(\mathbf{r} + \mathbf{R}) + \rho''_{1,0}^{ind}(\mathbf{r} + \mathbf{R}), \quad (A 19)$$

we find

$$\tilde{\rho}_1(\mathbf{k}) + \tilde{\rho}_{1,0}^{ind}(\mathbf{k}) = e^{-i\mathbf{kR}} [\tilde{\rho}'_1(\mathbf{k}) + \tilde{\rho}''_{1,0}^{ind}(\mathbf{k})]. \quad (A 20)$$

Taking into account that

$$\tilde{\rho}'(\mathbf{k}) = \frac{1}{(2\pi)^{3/2}} \int d^3\mathbf{r}' \rho'(\mathbf{r}') e^{i\mathbf{k}\mathbf{r}'} = \frac{1}{(2\pi)^{3/2}} \int d^3\mathbf{r}'' \rho''(\mathbf{r}'') e^{i\mathbf{k}\mathbf{r}'}, \quad (\text{A 21})$$

and introducing an Euler rotation matrix \mathbf{T} ,

$$\mathbf{r}'' = \mathbf{T}\mathbf{r}' \quad (\text{A 22})$$

$$\mathbf{T} = \begin{bmatrix} 1 & 0 & 0 \\ 0 & \cos\psi & -\sin\psi \\ 0 & \sin\psi & \cos\psi \end{bmatrix} \quad (\text{A 23})$$

we obtain

$$\tilde{\rho}'(\mathbf{k}) = \frac{1}{(2\pi)^{3/2}} \int d^3\mathbf{r}'' \rho''(\mathbf{r}'') e^{i\mathbf{k}\mathbf{T}^{-1}\mathbf{r}''} = \frac{1}{(2\pi)^{3/2}} \int d^3\mathbf{r}'' \rho''(\mathbf{r}'') e^{i\mathbf{m}\mathbf{r}''} = \tilde{\rho}''(\mathbf{m}) \quad (\text{A 24})$$

where

$$\mathbf{m} = \mathbf{T}\mathbf{k} = \begin{bmatrix} k_x \\ k_y \cos\psi - k_z \sin\psi \\ k_y \sin\psi + k_z \cos\psi \end{bmatrix} \quad (\text{A 25})$$

From Eqs. (A 20) and (A 24) we find

$$\tilde{\rho}_1(\mathbf{k}) + \tilde{\rho}_{1,0}^{ind}(\mathbf{k}) = e^{-i\mathbf{k}\mathbf{R}} \left[\tilde{\rho}_1''(\mathbf{m}) + \tilde{\rho}_{1,0}^{ind''}(\mathbf{m}) \right] \quad (\text{A 26})$$

and by analogy with Eq. (A 18) we arrive at

$$\tilde{\rho}_1(\mathbf{k}) + \tilde{\rho}_{1,0}^{ind}(\mathbf{k}) = -\frac{e^{-iKR\cos(\phi_K)}}{(2\pi)^{1/2}} \sum_{n=-\infty}^{\infty} i^n \frac{\tilde{\sigma}_1(\mu_z, n) J_n(Ma) e^{-in\phi_M}}{\tilde{\kappa}_{\mu_z} [1 - \tilde{\beta}_n(\mu_z)] I_n(\tilde{\kappa}_{\mu_z} a) K'_n(\tilde{\kappa}_{\mu_z} a)} \quad (\text{A 27})$$

where the relationship between the cylindrical coordinates of the vectors $\mathbf{k}=(q,K,\phi_K)$ and $\mathbf{m}=(\mu_z, M, \phi_M)$ is given by

$$\mu_z = q \cos\psi + K \sin\phi_K \sin\psi, \quad (\text{A 28})$$

$$M = \sqrt{K^2 + q^2 - \mu_z^2}, \quad (\text{A 29})$$

$$\cos \phi_M = \frac{K}{M} \cos \phi_K, \quad (A 30)$$

and

$$\sin \phi_M = \frac{K \sin \phi_K \cos \psi - q \sin \psi}{M}. \quad (A 31)$$

3. INTERACTION BETWEEN MOLECULES WITH ARBITRARY SURFACE CHARGE PATTERNS

After substituting Eqs. (A 18), (A 27), and (A 2) into Eq. (A 5), we obtain

$$E_{\text{int}} \approx \frac{2}{\epsilon_s} \sum_{n,m=-\infty}^{\infty} i^{n-m} \int_0^{\infty} K dK \int_0^{2\pi} d\phi_K \int_{-\infty}^{\infty} \frac{dq}{|K^2 + \tilde{\kappa}_q^2|} \left[\frac{\tilde{\sigma}_1(\mu_z, n) \tilde{\sigma}_2(-q, -m) J_n(Ma) J_m(Ka) e^{-iKR \cos(\phi_K)} e^{-in\phi_M} e^{im\phi_K}}{\tilde{\kappa}_{\mu_z} \tilde{\kappa}_q |1 - \tilde{\beta}_n(\mu_z)| |1 - \tilde{\beta}_m(q)| K'_n(\tilde{\kappa}_{\mu_z} a) K'_m(\tilde{\kappa}_q a) I_n(\tilde{\kappa}_{\mu_z} a) I_m(\tilde{\kappa}_q a)} \right] \quad (A 32)$$

This expression relates the interaction Hamiltonian with the surface charge densities on any two crossed molecules regardless of the details of their surface charge patterns. This is a general expression, since it is applicable to interaction between rods with arbitrary surface charge distributions. However, it is not exact because it is based on the first order approximation for induced charge densities. This expression becomes exact in nonpolar media where $\epsilon_s = \epsilon_c = \epsilon$ and $\kappa = 0$. In this case, it has the form

$$E_{\text{int}} = \frac{2a^2}{\epsilon} \sum_{n,m=-\infty}^{\infty} i^{n-m} \int_0^{\infty} K dK \int_0^{2\pi} d\phi_K \int_{-\infty}^{\infty} \frac{dq}{|K^2 + q^2|} \left[\tilde{\sigma}_1(\mu_z, n) \tilde{\sigma}_2(-q, -m) J_n(Ma) J_m(Ka) e^{-iKR \cos(\phi_K)} e^{-in\phi_M} e^{im\phi_K} \right] \quad (A 33)$$

4. INTERACTION BETWEEN MOLECULES WITH HELICAL SURFACE CHARGE PATTERNS

After substitution of Eq. (6) into Eq. (A 32), we arrive at

$$E_{\text{int}} \approx \frac{8\pi^2 \sigma_0^2}{\epsilon_s} \sum_{n,m=-\infty}^{\infty} \int_0^{\infty} \frac{K dK}{|K^2 + \tilde{\kappa}_q^2|} \int_0^{2\pi} d\phi_K \int_{-\infty}^{\infty} dq \left[e^{-iKR \cos(\phi_K)} i^{n-m} e^{-in\phi_M} e^{im\phi_K} e^{ingz_1} e^{-imgz_2} \right] \times \left[\frac{\tilde{p}(\mu_z) \tilde{p}(-q) \delta(\mu_z + ng) \delta(q + mg) J_n(Ma) J_m(Ka)}{\tilde{\kappa}_{\mu_z} \tilde{\kappa}_q |1 - \tilde{\beta}_n(\mu_z)| |1 - \tilde{\beta}_m(q)| K'_n(\tilde{\kappa}_{\mu_z} a) K'_m(\tilde{\kappa}_q a) I_n(\tilde{\kappa}_{\mu_z} a) I_m(\tilde{\kappa}_q a)} \right] \quad (A 34)$$

The delta function, $\delta(q+mg)$, removes the integral over q . Simplifying the resulting expression, we find

$$\begin{aligned}
E_{\text{int}} \approx & \frac{8\pi^2\sigma_0^2}{\varepsilon_w |\sin \psi|} \sum_{n,m=-\infty}^{\infty} \int_0^{\infty} \frac{dK}{[K^2 + \kappa_m^2]} \\
& \times \frac{\tilde{p}(-ng)\tilde{p}(mg)J_n(Ma)J_m(Ka)}{\kappa_n \kappa_m [1 - \tilde{\beta}_n(n)g] [1 - \tilde{\beta}_m(mg)] K'_n(\kappa_n a) K'_m(\kappa_m a) I_n(\kappa_n a) I_m(\kappa_m a)} \\
& \times \int_0^{2\pi} d\phi_K \delta \left[\sin \phi_K + \frac{u_{n,m}(\psi)}{K} \right] \\
& \times \cos \left[KR \cos(\phi_K) + n\phi_M(\phi_K) - m\phi_K + (m-n)\frac{\pi}{2} - ngz_1 + mgz_2 \right]
\end{aligned} \tag{A 35}$$

where

$$u_{n,m}(\psi) = \frac{ng - mg \cos \psi}{\sin \psi} \tag{A 36}$$

and

$$\kappa_n = \sqrt{\kappa^2 + n^2 g^2} \tag{A 37}$$

Let us use the equality

$$\delta \left[\sin \phi_K + \frac{u_{n,m}(\psi)}{K} \right] = \frac{\Theta(K - |u_{n,m}(\psi)|)}{| \cos \phi_K |} \left[\delta(\phi_K - \phi_K^{\#}) + \delta(\phi_K - \pi + \phi_K^{\#}) \right], \tag{A 38}$$

where $\Theta(x)$ is the Heaviside step-function,

$$\Theta(x) = \begin{cases} 1, & x \geq 0 \\ 0, & x < 0 \end{cases} \tag{A 39}$$

and

$$\phi_K^{\#} = \arcsin \left(\frac{-u_{n,m}(\psi)}{K} \right) = \arctan \left(\frac{-u_{n,m}(\psi)}{\sqrt{K^2 - u_{n,m}^2(\psi)}} \right). \tag{A 40}$$

Using the expression for $\phi_M(\phi_K)$ (Eqs. (A 30),(A 31)), we find

$$\phi_M \circ \phi_K^\# = \arctan \left(\frac{u_{m,n}(\psi)}{\sqrt{K^2 - u_{n,m}^2(\psi)}} \right). \quad (A 41)$$

After we substitute Eqs. (A 38), (A 41) into Eq. (A 35), introduce a new variable

$$t = \sqrt{K^2 - u_{n,m}^2(\psi)}, \quad (A 42)$$

and calculate the integral over ϕ_K , we obtain

$$E_{\text{int}} \approx \frac{8\pi^2 \sigma_0^2}{\epsilon_w |\sin \psi|} \sum_{n,m=-\infty}^{\infty} \frac{\int_{-1}^1 \tilde{p}(-ng) \tilde{p}(mg) \cos[n g z_1 - m g z_2] \mathbf{I}_{n,m}}{\kappa_n \kappa_m [1 - \tilde{\beta}_n(n g)] [1 - \tilde{\beta}_m(m g)] K'_n(\kappa_n a) K'_m(\kappa_m a) I_n(\kappa_n a) I_m(\kappa_m a)}, \quad (A 43)$$

where

$$\begin{aligned} \mathbf{I}_{n,m} = & 2 \int_0^\infty dt \frac{J_n \left[a \sqrt{t^2 + u_{m,n}^2(\psi)} \right] J_m \left[a \sqrt{t^2 + u_{n,m}^2(\psi)} \right]}{\left(t^2 + u_{n,m}^2(\psi) + \kappa_m^2 \right)} \\ & \times \cos \left[R t + n \arctan \left(\frac{u_{m,n}(\psi)}{t} \right) + \frac{\pi}{2} \right] + m \arctan \left(\frac{u_{n,m}(\psi)}{t} \right) + \frac{\pi}{2} \right], \end{aligned} \quad (A 44)$$

Now we are left with one integral which can be calculated by the contour integration technique after analytic continuation of the integrand as a function of t to the complex plane.

Calculation of $\mathbf{I}_{n,m}$ by contour integration

On the complex plane, the integrand in Eq. (A 44) has a pole at $t = \pm i \sqrt{u_{n,m}^2(\psi) + \kappa_m^2}$ and several branching points. The latter can be removed after a set of exact transformations of the integral. These transformations are different for zero and nonzero values of $u_{n,m}(\psi)$.

First, consider the case when both $u_{n,m}(\psi) \neq 0$ and $u_{m,n}(\psi) \neq 0$. In order to remove a branching point at $t=0$, we use the identity

$$\arctan \left(\frac{u_{n,m}(\psi)}{t} \right) = -\arctan \left(\frac{t}{u_{n,m}(\psi)} \right) + \text{sgn}(u_{n,m}(\psi)) \frac{\pi}{2}, \quad (A 45)$$

where the sign function is defined as

$$\operatorname{sgn} x = \begin{cases} \frac{x}{|x|}, & x \neq 0 \\ 1, & x = 0 \end{cases} . \quad (\text{A 46})$$

Then,

$$\mathbf{I}_{n,m} = \int_{-1}^{\frac{n[1+\operatorname{sgn}[u_{m,n}(\psi)]]+m[1+\operatorname{sgn}[u_{n,m}(\psi)]]}{2}} \tilde{\mathbf{I}}_{n,m}, \quad (\text{A 47})$$

where

$$\begin{aligned} \tilde{\mathbf{I}}_{n,m} = & \int_{-\infty}^{\infty} dt \frac{J_n[a\sqrt{t^2 + u_{m,n}^2(\psi)}]J_m[a\sqrt{t^2 + u_{n,m}^2(\psi)}]}{[t^2 + u_{n,m}^2(\psi) + \kappa_m^2]} \\ & \times \cos[Rt - n \arctan\left(\frac{t}{u_{m,n}(\psi)}\right) - m \arctan\left(\frac{t}{u_{n,m}(\psi)}\right)], \end{aligned} \quad (\text{A 48})$$

Since $\arctan(x)$ is an odd function of x and $\cos(x)$ is an even function of x , Eq. (A 48) can be rewritten in the following form

$$\begin{aligned} \tilde{\mathbf{I}}_{n,m} = & \int_{-\infty}^{\infty} dt \frac{J_n[a\sqrt{t^2 + u_{m,n}^2(\psi)}]J_m[a\sqrt{t^2 + u_{n,m}^2(\psi)}]}{[t^2 + u_{n,m}^2(\psi) + \kappa_m^2]} \\ & \times e^{iRt} e^{-in \arctan\left(\frac{t}{u_{m,n}(\psi)}\right)} e^{-im \arctan\left(\frac{t}{u_{n,m}(\psi)}\right)} \end{aligned} . \quad (\text{A 49})$$

Taking into account that

$$\arctan x = \frac{i}{2} \ln \frac{1-ix}{1+ix}, \quad (\text{A 50})$$

we find

$$\tilde{\mathbf{I}}_{n,m} = \int_{-\infty}^{\infty} \Delta_{n,m} dt \quad (\text{A 51})$$

where

$$\Delta_{n,m} \Big|_t = e^{iRt} \frac{J_n \left[a \sqrt{t^2 + u_{m,n}^2(\psi)} \right] J_m \left[a \sqrt{t^2 + u_{n,m}^2(\psi)} \right]}{\left[t^2 + u_{n,m}^2(\psi) + \kappa_m^2 \right]} \frac{\left| -i \frac{t}{u_{m,n}(\psi)} \right|^{\frac{n}{2}}}{\left| +i \frac{t}{u_{m,n}(\psi)} \right|^{\frac{n}{2}}} \frac{\left| -i \frac{t}{u_{n,m}(\psi)} \right|^{\frac{m}{2}}}{\left| +i \frac{t}{u_{n,m}(\psi)} \right|^{\frac{m}{2}}}. \quad (\text{A 52})$$

In $\Delta_{n,m} \Big|_t$, the J_n and J_m Bessel functions have branching points at $t = \pm iu_{m,n}(\psi)$. However, these branching points are compensated by the corresponding branching points of

$\left[\left| iu_{m,n}(\psi) + t \right| \right]^{\frac{n}{2}}$ and $\left[\left| iu_{n,m}(\psi) + t \right| \right]^{\frac{m}{2}}$. Therefore,

$$\tilde{\mathbf{I}}_{n,m} = 2\pi i \operatorname{Res} \left| \Delta_{n,m} \right|_{t=i\sqrt{u_{n,m}^2(\psi) + \kappa_m^2}}. \quad (\text{A 53})$$

Hence, we obtain

$$\tilde{\mathbf{I}}_{n,m} = \pi e^{-R\sqrt{u_{n,m}^2(\psi) + \kappa_m^2}} \frac{J_n \left[ia\kappa_n \right] J_m \left[ia\kappa_m \right]}{\sqrt{u_{n,m}^2(\psi) + \kappa_m^2}} \frac{\left| + \frac{\sqrt{u_{m,n}^2(\psi) + \kappa_n^2}}{u_{m,n}(\psi)} \right|^{\frac{n}{2}}}{\left| - \frac{\sqrt{u_{m,n}^2(\psi) + \kappa_n^2}}{u_{m,n}(\psi)} \right|^{\frac{n}{2}}} \frac{\left| + \frac{\sqrt{u_{n,m}^2(\psi) + \kappa_m^2}}{u_{n,m}(\psi)} \right|^{\frac{m}{2}}}{\left| - \frac{\sqrt{u_{n,m}^2(\psi) + \kappa_m^2}}{u_{n,m}(\psi)} \right|^{\frac{m}{2}}}. \quad (\text{A 54})$$

Since

$$\left| \pm \frac{\sqrt{u_{m,n}^2(\psi) + \kappa_n^2}}{u_{m,n}(\psi)} \right|^{\frac{n}{2}} = (-1)^{\frac{n[1-\operatorname{sgn}[u_{m,n}(\psi)]]}{4}} \frac{\left[\sqrt{u_{m,n}^2(\psi) + \kappa_n^2} \pm u_{m,n}(\psi) \right]^{\frac{n}{2}}}{|u_{m,n}(\psi)|^{\frac{n}{2}}}, \quad (\text{A 55})$$

we get

$$\begin{aligned} \tilde{\mathbf{I}}_{n,m} &= \pi (-1)^{\frac{n[1-\operatorname{sgn}[u_{m,n}(\psi)]]+m[1-\operatorname{sgn}[u_{n,m}(\psi)]]}{2}} e^{-R\sqrt{u_{n,m}^2(\psi) + \kappa_m^2}} \frac{I_n \left[a\kappa_n \right] I_m \left[a\kappa_m \right]}{\sqrt{u_{n,m}^2(\psi) + \kappa_m^2}} \\ &\times \frac{\left| \sqrt{u_{m,n}^2(\psi) + \kappa_n^2} + u_{m,n}(\psi) \right|^{\frac{n}{2}}}{\left| \sqrt{u_{m,n}^2(\psi) + \kappa_n^2} - u_{m,n}(\psi) \right|^{\frac{n}{2}}} \frac{\left| \sqrt{u_{n,m}^2(\psi) + \kappa_m^2} + u_{n,m}(\psi) \right|^{\frac{m}{2}}}{\left| \sqrt{u_{n,m}^2(\psi) + \kappa_m^2} - u_{n,m}(\psi) \right|^{\frac{m}{2}}}. \end{aligned} \quad (\text{A 56})$$

At $\cos\psi=n/m$, $u_{n,m}(\psi)=0$ while at $\cos\psi=m/n$, $u_{m,n}(\psi)=0$. Eq. (A 45) cannot be used at $u_{n,m}(\psi)=0$ or $u_{m,n}(\psi)=0$ ($u_{n,m}$ and $u_{m,n}$ cannot have zero values simultaneously at nonzero ψ). Consider, e.g., the case when $u_{n,m}(\psi)=0$ and $u_{m,n}(\psi)\neq 0$. Then,

$$\mathbf{I}_{n,m} = \int_{-1}^1 \int_{-1}^1 \frac{n[1+\operatorname{sgn}[u_{m,n}(\psi)]]}{2} \tilde{\mathbf{J}}_{n,m}, \quad (\text{A 57})$$

where

$$\tilde{\mathbf{J}}_{n,m} = \int_{-\infty}^{\infty} dt \frac{J_n[a\sqrt{t^2 + u_{m,n}^2(\psi)}] J_m[at]}{(t^2 + u_{n,m}^2(\psi) + \kappa_m^2)} \cos[Rt - n \arctan \frac{t}{u_{m,n}(\psi)} - m \frac{\pi}{2}] \quad (\text{A 58})$$

Here we used that the product of J_m and \cos in the integrand is an even function of t regardless of m . After performing the integration in the same way as above, we find that

$$\tilde{\mathbf{J}}_{n,m} = \tilde{\mathbf{I}}_{n,m} \quad (\text{A 59})$$

where $\tilde{\mathbf{I}}_{n,m}$ is still given by Eq. (A 56). Furthermore at $u_{n,m}(\psi)=0$, within our definition of $\operatorname{sgn}(x)$, $m[1+\operatorname{sgn}[u_{n,m}(\psi)]]/2 = m$.

Thus, whether $u_{n,m}$ or $u_{m,n}$ have zero values or not, we end up with the same result for $\mathbf{I}_{n,m}$ which is

$$\begin{aligned} \mathbf{I}_{n,m} = & \pi \int_{-1}^1 \int_{-1}^1 e^{-R\sqrt{u_{n,m}^2(\psi) + \kappa_m^2}} \frac{I_n[a\kappa_n] I_m[a\kappa_m]}{\sqrt{u_{n,m}^2(\psi) + \kappa_m^2}} \\ & \times \frac{\sqrt{u_{m,n}^2(\psi) + \kappa_n^2} + u_{m,n}(\psi)}{\sqrt{u_{m,n}^2(\psi) + \kappa_n^2} - u_{m,n}(\psi)} \frac{\sqrt{u_{n,m}^2(\psi) + \kappa_m^2} + u_{n,m}(\psi)}{\sqrt{u_{n,m}^2(\psi) + \kappa_m^2} - u_{n,m}(\psi)}. \end{aligned} \quad (\text{A 60})$$

After substitution of Eq. (A 60) into Eq. (A 43) we arrive at the formula for the interaction energy given by Eq. (9).

5. INTERACTION BETWEEN TWO HELICES WITH PARALLEL LONG AXES

At $\psi=0$, we find that $M=K$, $\mu_z=q$, $\phi_{\mathbf{M}}=\phi_{\mathbf{K}}$. Then, after integrating over $\phi_{\mathbf{K}}$ and subsequently over K , Eq. (A 32) takes the form

$$E_{\text{int}} \approx \frac{4\pi}{\epsilon_s} \sum_{n,m=-\infty}^{\infty} \int_{-\infty}^{\infty} \frac{\tilde{\sigma}_1(q,n) \tilde{\sigma}_2(-q,-m) K_{n-m}(\tilde{\kappa}_q R) dq}{\tilde{\kappa}_q^2 [1 - \tilde{\beta}_n(q)] [1 - \tilde{\beta}_m(q)] K'_n(\tilde{\kappa}_q a) K'_m(\tilde{\kappa}_q a)}, \quad (\text{A 61})$$

For infinitely long parallel molecules, the total energy of interaction at $\psi=0$ is, of course, infinite and the integral in Eq. (A 61) diverges. In this case, the meaningful value is the energy of interaction per unit length, which can be calculated as $\lim_{L \rightarrow \infty} \langle E_{\text{int}} \rangle / L$, where L is the length of the molecules. Then, it is convenient to introduce the charge density pair correlation function

$$s_{1,2}(q, n, m) = \lim_{L \rightarrow \infty} \left\langle \frac{\tilde{\sigma}_1(q, n) \tilde{\sigma}_2(-q, -m) + \tilde{\sigma}_1(-q, -n) \tilde{\sigma}_2(q, m)}{2L} \right\rangle. \quad (\text{A 62})$$

Within our definition of the Fourier transform, $\tilde{\sigma}_1(q, n) \tilde{\sigma}_2(-q, -m) / L$ does not depend on L at $L \rightarrow \infty$ and $\int_{-\infty}^{\infty} s_{1,2}(q, n, m) dq$ has a finite value [24]. Then, the energy per unit length of the molecules is given by

$$\frac{E_{\text{int}}}{L} \approx \frac{4\pi}{\epsilon_s} \sum_{n, m=-\infty}^{\infty} (-1)^{n+m} \int_{-\infty}^{\infty} \frac{s_{1,2}(q, n, m) K_{n-m}(\tilde{\kappa}_q R) dq}{\tilde{\kappa}_q^2 [1 - \tilde{\beta}_n(q)] [1 - \tilde{\beta}_m(q)] K'_n(\tilde{\kappa}_q a) K'_m(\tilde{\kappa}_q a)} \quad (\text{A 63})$$

For $\tilde{\beta}_n(q) \ll 1$, this expression reduces to our previous result [24], derived for $\epsilon_c / \epsilon_s \ll 1$.

- [1] F. Livolant, *J. Physique (Paris)*, **47**, 1605 (1986).
- [2] T.E. Strzelecka and R.L. Rill, *J. Am. Chem. Soc.*, **109**, 4513 (1987).
- [3] T.E. Strzelecka, M.W. Davidson, and R.L. Rill, *Nature*, **331**, 457 (1988).
- [4] Yu.M. Yevdokimov, S.G. Skurdin, and V.I. Salyanov, *Liq. Cryst.*, **3**, 1443 (1988).
- [5] F. Livolant, *Physica A*, **176**, 117 (1991).
- [6] A. Leforestier and F. Livolant, *Biophys. J.*, **65**, 56 (1993).
- [7] C. Robinson, *Tetrahedron*, **13**, 219 (1961).
- [8] D.B. Dupre and R.W. Duke, *J. Chem. Phys.*, **63**, 143 (1975).
- [9] M.M. Giraud-Guille, *Int. Rev. Cyt.*, **166**, 59 (1996).
- [10] D.H. Van Winkle, M.W. Davidson, W.-H. Chen, and R.L. Rill, *Macromolecules*, **23**, 4140 (1990).
- [11] R. Podgornik, H. Strey, and V.A. Parsegian, *Curr. Opinion Coll. Interface Sci.*, **3**, 534 (1998).
- [12] H.H. Strey, J. Wang, R. Podgornik, A. Rupprecht, L. Yu, V.A. Parsegian, and E.B. Sirota, submitted to *Phys. Rev. Lett.*
- [13] R.D. Kamien, *Mol. Cryst. Liq. Crys. A*, **299**, 265 (1997).
- [14] A.B. Harris, R.D. Kamien, and T.C. Lubensky, *Phys. Rev. Lett.*, **78**, 1476 (1997).
- [15] A.B. Harris, R.D. Kamien, and T.C. Lubensky, e-Print # 9901174 available from <http://xxx.lanl.gov>, *Condensed Matter* (1999).
- [16] T.C. Lubensky, A.B. Harris, R.D. Kamien, and G. Yan, *Ferroelectrics*, **212**, 1 (1998).
- [17] L. Onsager, *Ann. N. Y. Acad. Sci.*, **51**, 627 (1949).
- [18] S. L. Brenner and V. A. Parsegian, *Biophys. J.*, **14**, 327 (1974).
- [19] J.M. Bailey, *Biopolymers*, **12**, 559 (1973).
- [20] D. Soumpasis, *J. Chem. Phys.*, **69**, 3190 (1978).
- [21] B. Jayaram, K. A. Sharp, and B. Honig, *Biopolymers*, **28**, 975 (1989).
- [22] K. Wagner, E. Keyes, T. W. Kephart, and G. Edwards, *Biophys. J.*, **73**, 21 (1997).
- [23] B. Jayaram and D. L. Beveridge, *J. Phys. Chem.*, **94**, 4666 (1990).
- [24] A.A. Kornyshev and S. Leikin, *J. Chem. Phys.*, **107**, 3656 (1997); Erratum, *ibid.*, **108**, 7035 (1998).
- [25] A.A. Kornyshev and S. Leikin, *Biophys. J.*, **75**, 2513 (1998).
- [26] A.A. Kornyshev and S. Leikin, *Proc. Natl. Acad. Sci. USA*, **95**, 13579 (1998).
- [27] A.A. Kornyshev and S. Leikin, *Phys. Rev. Lett.*, **82**, 4138 (1999).
- [28] Such Hamiltonian includes both electrostatic and nonelectrostatic terms. Generally, the latter are not well known.
- [29] F. Oosawa, *Polyelectrolytes* (Marcel Dekker, New York, 1971).
- [30] J.L. Barrat and J.F. Joanny, *Adv. Chem. Phys.*, **94**, 1 (1996).
- [31] V.A. Bloomfield and I. Rouzina, *Methods Enzymol.*, **295**, 364 (1999).
- [32] We neglect dielectric saturation of the solvent in immediate vicinity of ions since we do not apply our results at such short distances. Furthermore, we do not account for nonlocal dielectric response of water and neglect hydration forces that may be caused by specific water ordering near molecular groups.
- [33] M.E. Fisher and Y. Levin, *Phys. Rev. Lett.*, **71**, 3826 (1993).
- [34] B.P. Lee and M.E. Fisher, *Phys. Rev. Lett.*, **76**, 2906 (1996).
- [35] M.E. Fisher, *J. Stat. Phys.*, **75**, 1 (1994).
- [36] D.M. Zuckerman, M.E. Fisher, and B.P. Lee, *Phys. Rev. E*, **56**, 6569 (1997).
- [37] See, e.g., W. Saenger, *Principles of Nucleic Acid Structure*, (Springer-Verlag, New York, 1984)
- [38] C.G. Baumann, S.B. Smith, V.A. Bloomfield, and C. Bustamante, *Proc. Natl. Acad. USA*, **94**, 6185 (1997).
- [39] Note that the spiral line running in the center of the minor groove crosses the (x'', z'') semi-plane at many points $z_l^{(k)}$ where $z_l^{(k)} = z_l + kH$ and k is an arbitrary integer. Any one of these points can be used

to define z_1 . Correspondingly, the interaction energy depends on z_1 and z_2 as $\cos(n g z_1 - m g z_2)$, where $gH=2\pi$, (see Eq. (9)). It is, therefore, invariant with respect to the $z_1^{(k)} = z_1 + kH$ transformation.

[40] Based on the crystallographic data [37] the deviation of the axial rise per base pair (bp) from its average value 3.34 Å is about 0.1 Å. For 150 bp -long DNA with random base pair sequence, this leads to axial deviation from the ideal helix $\sim 0.1 \text{ \AA} \times \sqrt{150} \approx 1.2 \text{ \AA}$ that is negligibly small compared to the helical pitch $H \approx 34 \text{ \AA}$. Similarly, the deviation of the helical twist angle from its average value 36 deg is $\sim 4 \text{ deg}$. The deviation over the whole length of the molecule is, therefore, $\sim 50 \text{ deg}$, which is still small enough compared to the full 360 deg turn that would disrupt orientational correlations between strands on opposing molecules.

[41] The average distance between neighboring charges on DNA surface is $\sim 7 \text{ \AA}$, much smaller than the helical pitch and than the separation between molecules in the cholesteric phase. Even when the molecules are in direct contact with each other, the effects from charge discreteness contribute only $\sim 10\%$ to the interaction energy [26]. In the cholesteric phase, their contribution should be much smaller.

[42] Eq. (17) differs from the result reported in Ref. 18 by a factor of two due to a misprint there (V.A. Parsegian, private communication).

[43] The radius of the cylinder formed by centers of phosphate groups on *B*-DNA is $a \approx 9 \text{ \AA}$.

[44] The distance range where this approximation is valid depends on the symmetry of molecular charge pattern that determines the "weight-factors" $p(n g)$. For example, when $p(n g) \ll p(g)$ at all $n > 1$, this approximation is valid at all separations. In contrast, when $p(g) = 0$, this approximation cannot be used at all.

[45] In Eq. (43) we used that zero surface-to-surface separation corresponds to $R = 2a$.

[46] In principle, one can describe intermediate angles by introducing a formula for $L_n(\psi)$ that interpolates between Eq. (25) at $|\psi| > \psi_0$ ($L_n > L$) and $L_n = L$ at $\psi = 0$.

[47] D. Durand, J. Doucet, and F. Livolant, *J. Phys. II France*, **2**, 1769 (1992).

[48] G.S. Manning, *Q. Rev. Biophys.*, **11**, 179 (1978).

[49] Since molecular packing in the cholesteric phase is nearly hexagonal, the distance between neighboring layers is $\sqrt{3}R/2$. The rotation per layer is ψ . The pitch corresponds to the rotation by 2π .

[50] L Salem, X. Chapuisat, G. Segal, P.C. Hiberty, C. Minot, C. Leforestier, P. Sautet, *J. Am. Chem. Soc.* **109**, 2887 (1987).

[51] P.G. de Gennes and J. Prost, *The Physics of Liquid Crystals* (Clarendon Press, Oxford, 1993).

[52] R. Podgornik, H.H. Strey, K. Gawrisch, D.C. Rau, A. Rupprecht, and V.A. Parsegian, *Proc. Natl. Acad. Sci. USA*, **93**, 4261 (1996).

[53] As shown above, this condition is sufficient for existence of nonzero macroscopic torque between molecular layers. Here, for heuristic purposes, we select the simplest possible model and assume that this is also a necessary condition. The latter may or may not be true. Only a more detailed theory can answer this question.

[54] F. Livolant and M.F. Maestre, *Biochemistry*, **27**, 3056 (1988).

[55] G. Maret, M. Milas, and M. Rinaudo, *Polym. Bull.*, **4**, 291 (1981).

[56] Note that for biological helices immersed into an aqueous electrolyte solution $|\tilde{\beta}_m(q)| \ll 1$ because $\epsilon_c/\epsilon_s \ll 1$. In this case, Eq. (A 16) can be simplified to yield

$$\tilde{\sigma}_2(q, m) + \tilde{\sigma}_{2,0}^{ind}(q, m) \approx - \frac{\tilde{\sigma}_2(q, m)}{\tilde{\kappa}_q a I_m(\tilde{\kappa}_q a) K'_m(\tilde{\kappa}_q a)}$$

We used this result in our previous work [24]. However, here we will also discuss interactions between macromolecules in nonpolar media when $\epsilon_c=\epsilon_s$ and $\kappa=0$. Then, such approximation cannot be used and, thus, we avoid it altogether.